



# Distinct Conformations, Aggregation and Cellular Internalization of Different Tau Strains

Thomas K. Karikari<sup>1,2\*</sup>, David A. Nagel<sup>3</sup>, Alastair Grainger<sup>3</sup>, Charlotte Clarke-Bland<sup>3</sup>, James Crowe<sup>3</sup>, Eric J. Hill<sup>3</sup> and Kevin G. Moffat<sup>1</sup>

<sup>1</sup> School of Life Sciences, University of Warwick, Coventry, United Kingdom, <sup>2</sup> Midlands Integrative Biosciences Training Partnership, University of Warwick, Coventry, United Kingdom, <sup>3</sup> School of Life and Health Sciences, Aston University, Birmingham, United Kingdom

## OPEN ACCESS

### Edited by:

Jesus Avila,  
Autonomous University of Madrid,  
Spain

### Reviewed by:

Diana Laura Castillo-Carranza,  
Hampton University, United States  
Sheng Zhang,  
University of Texas Health Science  
Center at Houston, United States

### \*Correspondence:

Thomas K. Karikari  
Thomas.Karikari@gu.se;  
ohenekakari@gmail.com

### † Present address:

Thomas K. Karikari,  
Department of Psychiatry  
and Neurochemistry, Institute  
of Neuroscience and Physiology,  
The Sahlgrenska Academy  
at the University of Gothenburg,  
Gothenburg, Sweden

### Specialty section:

This article was submitted to  
Cellular Neuropathology,  
a section of the journal  
Frontiers in Cellular Neuroscience

**Received:** 12 January 2019

**Accepted:** 18 June 2019

**Published:** 09 July 2019

### Citation:

Karikari TK, Nagel DA, Grainger A,  
Clarke-Bland C, Crowe J, Hill EJ and  
Moffat KG (2019) Distinct  
Conformations, Aggregation  
and Cellular Internalization of Different  
Tau Strains.  
*Front. Cell. Neurosci.* 13:296.  
doi: 10.3389/fncel.2019.00296

The inter-cellular propagation of tau aggregates in several neurodegenerative diseases involves, in part, recurring cycles of extracellular tau uptake, initiation of endogenous tau aggregation, and extracellular release of at least part of this protein complex. However, human brain tau extracts from diverse tauopathies exhibit variant or “strain” specificity in inducing inter-cellular propagation in both cell and animal models. It is unclear if these distinctive properties are affected by disease-specific differences in aggregated tau conformation and structure. We have used a combined structural and cell biological approach to study if two frontotemporal dementia (FTD)-associated pathologic mutations, V337M and N279K, affect the aggregation, conformation and cellular internalization of the tau four-repeat domain (K18) fragment. In both heparin-induced and native-state aggregation experiments, each FTD variant formed soluble and fibrillar aggregates with remarkable morphological and immunological distinctions from the wild type (WT) aggregates. Exogenously applied oligomers of the FTD tau-K18 variants (V337M and N279K) were significantly more efficiently taken up by SH-SY5Y neuroblastoma cells than WT tau-K18, suggesting mutation-induced changes in cellular internalization. However, shared internalization mechanisms were observed: endocytosed oligomers were distributed in the cytoplasm and nucleus of SH-SY5Y cells and the neurites and soma of human induced pluripotent stem cell-derived neurons, where they co-localized with endogenous tau and the nuclear protein nucleolin. Altogether, evidence of conformational and aggregation differences between WT and disease-mutated tau K18 is demonstrated, which may explain their distinct cellular internalization potencies. These findings may account for critical aspects of the molecular pathogenesis of tauopathies involving WT and mutated tau.

**Keywords:** tau protein, Alzheimer’s disease, frontotemporal dementia, MAPT mutations, oligomer, nuclear tau, cellular internalization, induced pluripotent stem cell-derived neurons

**Abbreviations:** AD, Alzheimer’s disease; ANOVA, analysis of variance; CBD, corticobasal degeneration; DPBS, Dulbecco’s phosphate buffered saline; EDTA, ethylenediaminetetraacetic acid; FTD, frontotemporal dementia; hiPSC-derived neurons, human induced pluripotent stem cell-derived cortical neurons; LMW, low molecular weight; MT, microtubule; NFT, neurofibrillary tangle; PHE, paired helical filaments; PIPES, piperazine-N,N’-bis(2-ethanesulfonic acid); SF, straight filament; TCEP, tris(2-carboxyethyl)phosphine; TEM, transmission electron microscopy; WT, wild type.

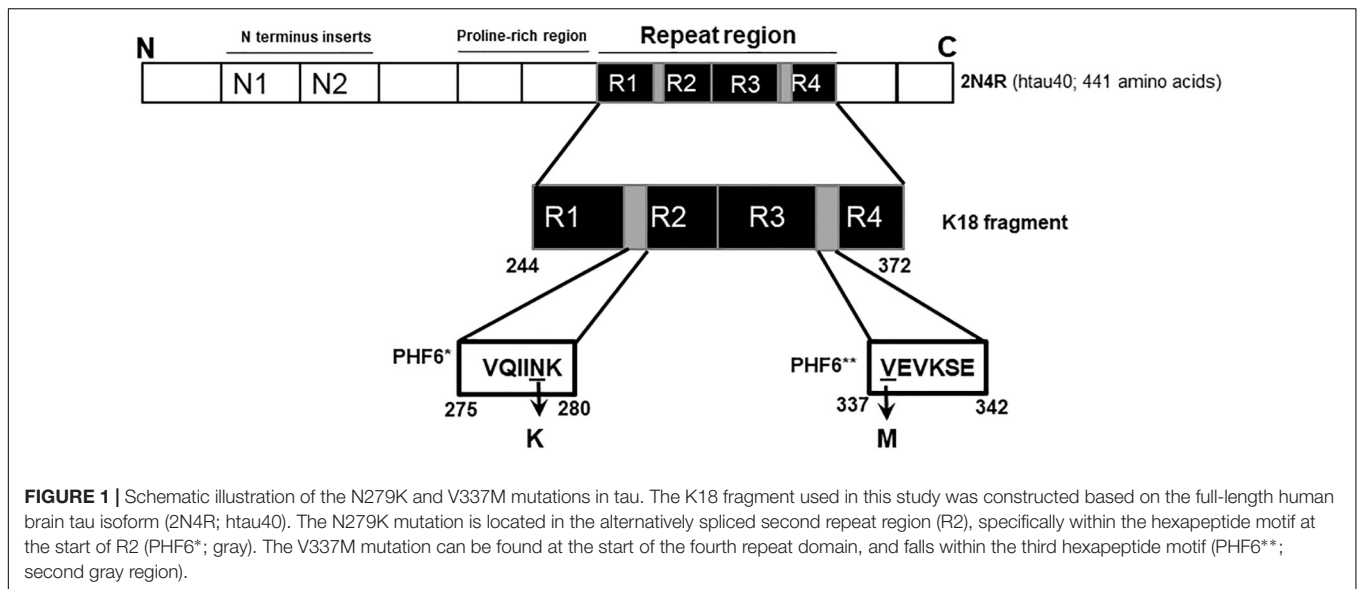
## INTRODUCTION

Tauopathies are characterized by the intracellular accumulation of NFTs composed of aggregated misfolded tau (Arriagada et al., 1992; Spillantini and Goedert, 2013). NFTs can be formed when tau proteins lose affinity for MTs and bind to themselves, forming insoluble aggregates that can subsequently develop into NFTs (Goedert, 2016). Although monomeric tau – the physiological form of the protein – is natively unfolded, it becomes progressively enriched in  $\beta$ -sheets through initial aggregation into soluble conformers and then into PHFs and NFTs (Barghorn et al., 2004; von Bergen et al., 2005). Although growing evidence indicates that tau dysfunction can cause neurodegeneration, the mechanisms involved are not well understood (Guo and Lee, 2014; Walsh and Selkoe, 2016). Many recent studies have shown that the typical temporal and spatial accumulation of tau inclusions in specific brain regions in AD and other tauopathies may be due to the propagation of aggregated tau between synaptically connected neurons (Frost et al., 2009; Guo and Lee, 2014; Usenovic et al., 2015). This inter-neuronal propagation of abnormal tau, often referred to as “spread,” is understood to initiate the structural and functional differences observed in affected brain regions (Boluda et al., 2015; Usenovic et al., 2015). As a predominantly cytosolic protein, the spread of tau is expected to involve repeated cycles of the following steps: (i) secretion of tau, either in aggregated or soluble forms, from donor neurons; (ii) uptake of extracellular tau into specific neighboring neurons; (iii) induction of endogenous tau aggregation in the recipient neurons; and (iv) the secretion of at least part of this internalized tau-endogenous tau protein complex (Clavaguera et al., 2009; Frost et al., 2009; Guo and Lee, 2011; Lasagna-Reeves et al., 2012a; Michel et al., 2014). Nonetheless, the molecular mechanism governing this process is poorly understood (Walsh and Selkoe, 2016). As such, an improved understanding of the pathways involved in these diseases could lead to the development of new therapies.

The efficiency of the inter-cellular propagation of pathological tau appears to be influenced by the conformations of both the seed (internalized) and the seeded (recipient endogenous) proteins (Goedert et al., 2014; Sanders et al., 2014; Wegmann et al., 2015; Alonso et al., 2016; Kaufman et al., 2016). This has therefore led to the *tau strain hypothesis*, which proposes that different aggregated tau conformers (distinct strains) will have distinct pathology-initiating capacities because they interact with endogenous tau differently (Sanders et al., 2014; Gerson et al., 2016). This hypothesis is supported by several studies (Clavaguera et al., 2013; Sanders et al., 2014; Boluda et al., 2015; Kaufman et al., 2016; Narasimhan et al., 2017; Strang et al., 2017). For example, intracerebral introduction of human tauopathy brain isolates into brains of the non-filament-forming ALZ17 mice led to distinctions in the induction of tau inclusions, dependent on the source of homogenate (Clavaguera et al., 2013). Inclusions formed after injecting isolates from human AD, progressive supranuclear palsy, argyrophilic grain disease, CBD or tangle-only dementia propagated between neighboring brain regions. Conversely, propagation was not observed for aggregates formed in the case of Pick's disease. Importantly, these

results were similar to those recorded after seeding WT mice with the same isolates, suggesting that the genetic background of the animals did not influence the outcome (Clavaguera et al., 2013). Similarly, intracerebral introduction of brain extracts from human CBD and AD cases into young tangle-forming PS19 mice brains resulted in the formation and propagation of tau inclusions and neuronal loss that appeared specific to selected cell types (Boluda et al., 2015). Extracts from CBD patients led to tau inclusions limited to oligodendrocytes of the fimbria and white matter around the injection site, while tau aggregates formed after introducing AD extracts were found in neuronal perikarya without obvious oligodendrocyte participation (Boluda et al., 2015). These results suggest that tau isolates from different sources can exhibit distinctions in their ability to induce tau inclusion formation in the recipient cell type, which may be due to conformational differences between the endogenous tau and the initiating tau seeds. Recently, both cell-type specificity and differential endogenous tau recruitment have been implicated as determinants of inter-cellular propagation of human tauopathy brain extracts (Narasimhan et al., 2017). Furthermore, recombinant full-length and truncated forms of tau, such as the four-repeat K18 region comprising residues 244–372 of full-length tau 441 (**Figure 1**), have been shown to initiate propagation by inducing endogenous tau aggregation (Guo and Lee, 2011; Iba et al., 2013; Michel et al., 2014; Falcon et al., 2015; Usenovic et al., 2015). This seeding capacity may be due to conformational similarities between some forms of recombinant tau applied as seeds and the endogenous tau, because these recombinant forms can take on endogenous tau conformation in some cell models (Falcon et al., 2015).

Whilst there is mounting data supporting the inter-cellular propagation of aggregated recombinant WT tau, we know little about FTD (Bodea et al., 2016). Many familial FTD cases are characterized by single point mutations in the *MAPT* gene, which encodes the tau protein. Specific FTD-associated *MAPT* mutations have been shown to alter the aggregation,  $\beta$ -sheet propensity, isoform ratio and MT binding properties of the WT tau (Hong et al., 1998; Barghorn et al., 2000; von Bergen et al., 2001; Combs and Gamblin, 2012; Kaniyappan et al., 2017). It is, however, unclear if aggregated tau proteins from FTD with *MAPT* mutations are conformationally distinct from WT tau, and if they have different cellular internalization behavior and colocalization dynamics with endogenous tau. Strang et al. (2017) recently demonstrated that the ability of exogenous WT tau K18 fibrils to induce aggregation in cells over-expressing tau carrying different FTD mutations is uniquely dependent on the specific mutation and its surrounding amino acid sequences. However, several questions remain, such as what structural features determine these distinct activities? Do the conformation and aggregation characteristics of tau variants influence their cellular internalization and endogenous tau interaction? Furthermore, it has been shown that the N279K variant of the tau 250–300 fragment localizes to the nucleus more efficiently than the WT when overexpressed in a mammalian cell line (Ritter et al., 2018). It is yet to be shown if exogenously applied aggregates of this and other FTD variants of tau can enter recipient cells and localize to the nucleus, in a process suggestive of



cell-to-cell propagation. Answering these questions is critical to understanding the mechanisms by which AD and non-AD tauopathies develop, and will help to establish if selectivity is required in drug development for treating tauopathies.

In this study, we investigated the *in vitro* conformation and aggregation of tau K18-WT and two FTD variants, namely V337M and N279K. The N279K mutation is a part of the PHF6\* hexapeptide motif (<sup>275</sup>VQIINK<sup>280</sup>) but the V337M mutation is located in the PHF6\*\* hexapeptide motif (<sup>337</sup>VEVKSE<sup>342</sup>) (Li and Lee, 2006; Grüning et al., 2014). Since these motifs critically regulate tau aggregation and seeding behavior, amino acid mutations were hypothesized to alter these processes (von Bergen et al., 2000, 2001; Li and Lee, 2006; Grüning et al., 2014; Falcon et al., 2015). In addition, the N279K and V337M are located in the second and the fourth MT binding repeat regions, respectively (Figure 1). Thus, the characterization of these mutations should offer new understanding into the consequences of disease-related alterations in alternatively- and constitutively spliced domains. The mutations also have distinct pathological consequences in human brains (Hong et al., 1998), suggesting differential effects on tau aggregation and structure.

We have shown that the structural morphology and immunoreactivity of K18-WT aggregation products were distinctively altered in the presence of each mutation. Furthermore, internalization of exogenous structurally defined oligomers into SH-SY5Y cells was significantly increased in the presence of each FTD mutation. However, the sub-cellular localization and endogenous tau co-localization patterns were similar between the three protein variants, both in SH-SY5Y cells and differentiated human induced pluripotent stem cell (hiPSC)-derived neurons. This may suggest shared mechanisms of cellular uptake, but differences in the efficiency of uptake, between WT tau K18 and its V337M and N279K FTD variants. Together, the results give new insights into the structural and functional dynamics of WT and FTD tau. We hypothesize that the distinct conformation and aggregation behaviors of the tau K18 variants may influence

their inter-cellular propagation characteristics. These findings may help to explain important aspects of similarities and heterogeneity in tauopathies involving WT and mutated tau.

## MATERIALS AND METHODS

### Materials

Heparin (#H3393), SH-SY5Y cells (#94030304), sodium chloride (#S/3160/60), sodium phosphate dibasic (#S9763-500 G), sodium phosphate monobasic dihydrate (#04269-1 KG), Triton X-100 (#X100-500 ML), Tween (#P9416-100 ML), F12 Ham (#51651C), L-Glutamine (#G7513), fetal bovine serum (#F2442) and antibiotic antimycotic acid (#A5955) were purchased from Sigma Aldrich, St. Louis, Missouri, United States. X1 Amersham Protran 0.45  $\mu$ m electrochemiluminescence nitrocellulose membrane (#15259794) and Amersham electrochemiluminescence system (#RPN2108) were obtained from GE Healthcare, Buckinghamshire, United Kingdom. EDTA (#D/0700/53) was bought from Fisher Scientific, Loughborough, United Kingdom. PIPES (#A16090) was bought from Alfa Aesar, Heysham, United Kingdom, whilst DMSO (cell culture-grade; #P60-36720100) was from PAN-Biotech GmbH, Aidenbach, Germany. CL-XPosure Film (#34089) and ProLong Gold antifade mounting medium (#P36934) were purchased from Thermo Fisher Scientific, Rockford, Illinois, United States. CellMask<sup>®</sup> Deep Red plasma membrane stain (#C10046), Hoechst 33342 (#H21492) and Alexa Fluor<sup>®</sup> 488 C5-maleimide (#A10254) were bought from Molecular Probes, Eugene, Oregon, United States. Lactate dehydrogenase (LDH) cytotoxicity assay kit (#88954) was obtained from Pierce Biotechnology, Rockford, Illinois, United States. TCEP (#A2233,0001) was procured from AppliChem GmbH, Damstadt, Germany. SynaptoRed<sup>™</sup> C2 (FM4-64; #70021) was obtained from Biotium Hayward, California, United States. CellView<sup>™</sup> dishes (#627975) were procured from Greiner Bio-One, Kremsmünster, Austria.

**TABLE 1** | Antibodies used in this study.

Antibody	Epitope	Host species	Vendor	Dilution
Primary antibodies				
Polyclonal rabbit anti-human tau (#A0024)	The MT binding repeat of tau	Rabbit	Dako	1:1000
T22 oligomeric tau (#ABN454)	Tau MT binding domain	Rabbit	Merck	1:1000
HT7 anti-human tau (#MN1000)	Amino acid sequence 159PPGQK <sup>163</sup> of full length human tau 2N4R	Mouse	Thermo Scientific	1:100
Alexa Fluor <sup>®</sup> 647-conjugated anti-nucleolin (#ab198580)	Human nucleolin	Mouse	Abcam	1:500
Secondary antibodies				
Goat anti-rabbit IgG (#31460)	–	Goat	Thermo Fisher Scientific	1:1000
Alexa Fluor <sup>®</sup> 594-conjugated AffiniPure goat anti-mouse	–	Goat	Jackson ImmunoResearch	1:100

Formvar/carbon-coated 300-mesh copper grids (#S162) and mica (#G250-3) were purchased from Agar Scientific, Stansted, Essex, United Kingdom. Neural precursor cells (#ax0016), Axol neural maintenance medium kit (#ax0031), and Surebond reagent (#ax0041) were purchased from Axol Bioscience, Little Chesterford, Cambridge, United Kingdom. Marvel dried skimmed milk was obtained from Premier Foods Company, United Kingdom. Antibodies used have been described in **Table 1**.

## Site Directed Mutagenesis, Protein Expression and Purification

Detailed description of the construction of the pProEx-HTa-Myc-K18 plasmid, and sequence-verified site-directed mutagenesis to create plasmid variants encoding the V337M and N279K mutations has been provided previously (Karikari et al., 2017). To prevent potential adverse functional effects of maleimide labeling, the native cysteines located in the central core of the MT binding region were each changed to alanine (C291A, C322A) and a new cysteine placed outside the central core of this region (I260C). These cysteine modifications were achieved by site-directed mutagenesis as described (Karikari et al., 2017). Several studies have used this approach, understood not to impact tau aggregation behavior, to study the biochemical properties and internalization of extracellular tau (Kumar et al., 2014; Michel et al., 2014; Shammas et al., 2015). The same cysteine-modified proteins were used in all experiments. Plasmids encoding N-terminal 6xHis-c-Myc K18-WT, K18-V337M and K18-N279K were expressed in BL21 (DE3)\*pRosetta *Escherichia coli*, purified with immobilized metal affinity chromatography and quantified with the Bicinchoninic acid assay as described previously (Karikari et al., 2017).

## Filament Assembly and Structural Characterization Using Negative-Stain Transmission Electron Microscopy (TEM)

K18-WT or its variants (38.5  $\mu$ M) mixed with 125  $\mu$ M heparin were incubated at 37°C without agitation for 4 or 45 days. Sodium phosphate buffer pH 7.4 was the diluent buffer used in all biochemical experiments unless otherwise indicated. All incubation was performed using an Eppendorf Mastercycler thermocycler, and aliquots removed for TEM. Five microliters of the indicated proteins were pipetted onto glow-discharged formvar/carbon-coated 300-mesh grids for 2 min, and filter paper strips used to remove unbound samples. Thereafter, 5  $\mu$ l of 2% uranyl acetate was added for 2 min, and the excess removed as previously before imaging. Quantitative analyses of filament lengths and widths were performed using Image J.

## Dot Blot Analysis of Protein Conformation

Protein variants at 55  $\mu$ M were incubated at 37°C to promote aggregation. Aliquots removed at the given times were snap-frozen and stored at –80°C until needed. After diluting samples 1:2, 2  $\mu$ l of the diluted samples were spotted onto 0.45- $\mu$ m nitrocellulose membrane, air-dried, blocked for 30 min at room temperature with 10% non-fat milk in phosphate buffered saline (PBS), and washed five times using 10% Tris buffered saline-0.05% Tween. The membrane was incubated for 2 h in anti-tau #A0024 or T22, washed as previously, and incubated with anti-rabbit immunoglobulin G (**Table 1**) for a further 2 h. Each antibody was diluted 1:1000. The membrane was then washed five times, developed using electrochemiluminescence reagents (Amersham), imaged and analyzed as previously described (Karikari et al., 2017).

## Preparation and Characterization of Labeled Oligomers

Proteins were treated with five times excess of TCEP for 1 h, and then treated with 4 $\times$  Alexa Fluor 488-C5-maleimide in the presence of 1 $\times$  BRB buffer (1 mM KCl, 80 mM PIPES, and 1 mM EDTA pH 6.8). Free fluorophore was dialyzed out against dialysis buffer (50 mM Tris HCl pH 7.5, 100 mM NaCl) in Slide-A-Lyzer MINI Dialysis Device (5 K MWCO; Thermo Fisher Scientific) with punctured buffer reservoirs placed in containers that can hold 2 L of dialysis buffer. The buffer was changed every 2 h with a total of five buffer replacements. Labeling was confirmed using non-denaturing sodium dodecyl sulfate-polyacrylamide gel electrophoresis followed by ultraviolet light exposure. The efficiency of labeling was routinely estimated using Beer's law and the molar extinction coefficient of 72,000/cm/M for Alexa Fluor 488-C5-maleimide.

## SH-SY5Y Cell Culture

SH-SY5Y cells were cultured on 1:1 minimal essential medium/F12 Ham medium supplemented with 1% L-Glutamine, 15% fetal bovine serum, and 1% antibiotic antimycotic acid (10,000 units penicillin, 10 mg streptomycin and 25  $\mu$ g amphotericin B). All experiments were performed using cells between passages two

and ten. Cells were grown at a density of 200,000 cells/ml in CellView™ dishes, 10  $\mu$ M labeled tau oligomers added to the medium, and incubated for 24 h at 37°C, 5% CO<sub>2</sub>. After removing the used medium, the cells were washed with warm PBS and fresh medium with 2  $\mu$ M Hoechst and 1:1000 dilution of CellMask Deep Red added before imaging.

## hiPSC-Derived Neuronal Culture

Neural precursors – from cord blood CD34+ cells of a newborn female – that had been cultured for 21 days from iPSCs to neural precursor cells were bought from Axol Bioscience. Grade 12-well tissue culture plates (Corning, New York, United States) or plates containing plasma-cleaned and ethanol-sterilized 13 mm glass coverslips (Menzer, Thermo Fisher Scientific) were each pre-coated with 250  $\mu$ l/cm<sup>2</sup> ReadySet reagent (Axol Bioscience) and kept at 37°C, 5% CO<sub>2</sub> for 45 min. The plates were then rinsed 4× with double-distilled water. Thereafter, Surebond reagent (Axol Bioscience) diluted in DPBS was added to the plates at 200  $\mu$ l/cm<sup>2</sup> and kept at 37°C, 5% CO<sub>2</sub> for at least 1 h. Cells were seeded on plasma-cleaned 13 mm glass coverslips at 25,000 cells/cm<sup>2</sup> final density and stored at 37°C, 5% CO<sub>2</sub>. The media was changed every other day for 14–16 days using the Axol Neural Maintenance Medium kit (#ax0031, Axol Bioscience). Phase contrast microscopy images taken periodically with the EVOS XL Core Imaging System (Life Technologies) and the expression of neuron-specific markers (data not shown) were used to monitor neuronal differentiation. Tau K18 oligomers diluted to 5  $\mu$ M in neural maintenance medium were applied to cultured neurons and kept at 37°C, 5% CO<sub>2</sub> for 24 h, after which the used medium was carefully removed and the neurons washed with DPBS before the addition of fresh medium.

## Immunocytochemistry

SH-SY5Y cells: the appropriate antibodies or dye were applied to the cells as described above and images taken with confocal microscopy without fixing. In internalization analysis, fresh media containing FM4-64 (2  $\mu$ M) and Hoechst was added to cells after PBS wash as explained above. The cells were imaged after 30 min incubation at 37°C and 5% CO<sub>2</sub>. Nucleolin co-localization was investigated by adding a 500× dilution of an Alexa Fluor-647-labeled anti-human nucleolin (Table 1) in tau-free medium to tau oligomer-treated cells after PBS wash as described above. Cells were imaged after 2 h incubation at 37°C and 5% CO<sub>2</sub>. Cells were imaged without fixing.

hiPSC-derived neurons: Neurons were fixed with 4% paraformaldehyde for 30 min, twice washed with DPBS and then cleaned with permeabilizing solution (0.2% Triton in DPBS). Thereafter, the fixed neurons were stored in blocking buffer (DPBS containing 0.2% Triton and 2% BSA) for 1 h. Subsequently the cells were incubated with primary antibody and Hoechst for 1 h at 37°C and 5% CO<sub>2</sub>. The fixed neurons were washed thrice, each for 5 min, with blocking buffer to remove unbound primary antibody and then incubated for 1 h with secondary antibody diluted in blocking buffer. After incubation with the secondary antibody, the wash steps were repeated. The prepared coverslips were rinsed with distilled water and slide-mounted with ProLong Gold antifade mounting medium.

Slides were incubated in the dark for at least 24 h before imaging. Details of antibodies used are available in Table 1.

## Confocal Microscopy

An LSM 710 (Leica) equipped with an C-Apochromat 63×/1.20 W Korr M27 objective lens was used to image SH-SY5Y cells. hiPSC-derived cortical neurons were imaged with the 63× objective of a Leica STP 6000 microscope. Images were analyzed with Image J. Internalization data are expressed as integrated density (area × mean fluorescent intensity). Identical imaging settings were used for each set of experiments (at least  $n = 3$ ).

## LDH Assay

The Pierce LDH cytotoxicity assay kit was used. SH-SY5Y cells were seeded at 20,000 cells/well in Falcon 96-well plates and the indicated oligomer concentrations added. Controls included spontaneous cytotoxicity (cells + 10  $\mu$ l sterile water), media only (no cells) and maximum control (membrane lysed with a manufacturer-supplied reagent). Cells were incubated for 72 h at 37°C 5% CO<sub>2</sub>. After incubation, lysis buffer was added to the maximum control wells and the plate incubated for a further 45 min. An aliquot (50  $\mu$ l) of the sample mix in each well was transferred to a new 96-well plate and 50  $\mu$ l reaction mix from the kit added to each well before incubation in the dark for 30 min. Stop solution (50  $\mu$ l) was added and absorbance measured at 490 and 680 nm. Background readings at 680 nm were subtracted from corresponding 490 nm readings and LDH release (cytotoxicity) for each condition calculated by dividing that condition's LDH activity value by the value for the maximum LDH activity control, and subtracting the spontaneous LDH activity value from both the numerator and the denominator.

## Statistics

Statistical analysis was done using Prism 6 (GraphPad Inc., CA, United States) at 95% confidence interval. The D'Agostino and Pearson test was used to test the datasets for normality. Whenever appropriate, parametric analysis was performed using one-way ANOVA with Tukey's *post hoc* test. Conversely, non-parametric datasets were analyzed using Kruskal–Wallis test with Dunn's *post hoc* test. Data are shown as mean  $\pm$  standard error of the mean.

## RESULTS

The K18 fragment consists of residues critical for tau aggregation and conformation, including the hexapeptide motifs at the beginning of repeat domains two (<sup>275</sup>VQIINK<sup>280</sup>), three (<sup>306</sup>VQIVYK<sup>311</sup>), and four (<sup>337</sup>VEVKSE<sup>342</sup>) (Figure 1). These motifs control aggregation by modulating tau-tau interactions that lead to conformational changes from random coil to cross  $\beta$ -sheet structures (von Bergen et al., 2000, 2005; Li and Lee, 2006; Grüning et al., 2014). Moreover, protomers comprising residues 306–378 form the core of tau filaments, with their differential packing mechanisms determining the type of aggregates formed

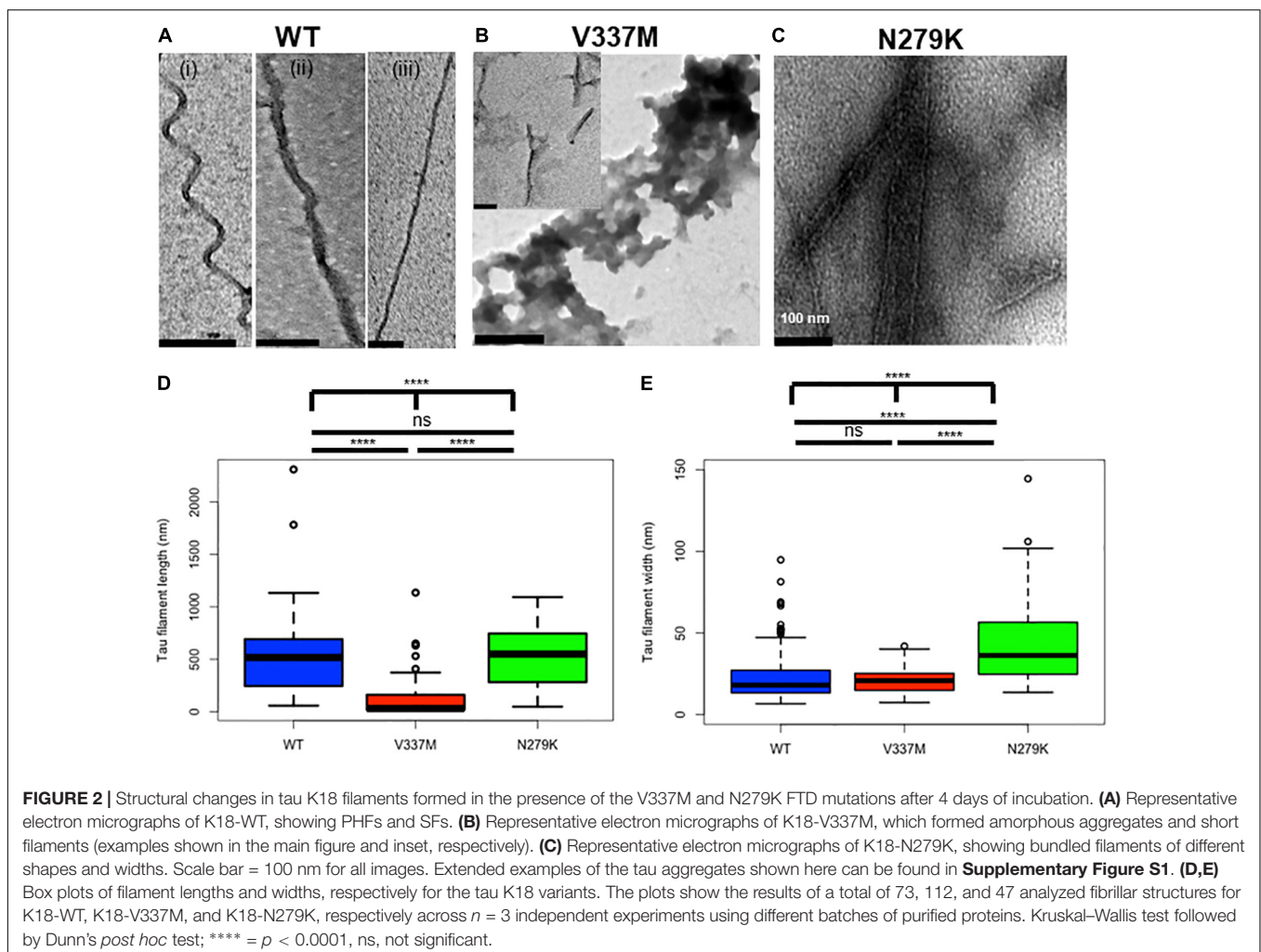
(Fitzpatrick et al., 2017). Furthermore, the protein's aggregation-seeding competence, partly responsible for its inter-cellular propagation, is held in the repeat region and its fragments consisting of specific motifs (Guo and Lee, 2011; Michel et al., 2014; Stöhr et al., 2017). As the repeat region contains residues that control tau aggregation, conformation and propagation, the K18 fragment was used to study potential effects of specific FTD mutations on these properties.

### Familial FTD Mutations Alter the Ultra-Structure of Tau K18 Aggregates

Negative-stain TEM was used to study effects of the N279K and V337M mutations on tau K18 aggregation. Each sample was incubated with heparin at 37°C for four days (96 h) before TEM analysis. After this aggregation period, K18-WT mostly formed PHFs and, to a lesser degree, SFs. Both phenotypes of K18-WT have been reported previously (Barghorn and Mandelkow, 2002). The PHFs had different degrees of twisting, which increased up to ~45° (Figure 2A and Supplementary Figure S1A). Unlike the PHFs, the SFs had no obvious helical structures (Figure 2Aiii). Tau K18-V337M aggregates had two types of

phenotypes: large amorphous aggregates (Figure 2B main image) and short filamentous aggregates (Figure 2B inset). On the other hand, K18-N279K formed thick bundles of filaments of various width and length (Figure 2C). Supplementary Figure S1 is an extension of Figure 2, showing representative images from  $n = 3$  independent experiments using different batches of purified proteins which further demonstrate the variety of aggregates formed by each tau K18 variant.

Filament length was significantly different when comparing all three proteins ( $p < 0.0001$ , Kruskal-Wallis test; mean lengths =  $510.8 \pm 42.3$  nm,  $106.6 \pm 15.4$  nm, and  $534.8 \pm 42.9$  nm for WT, V337M, and N279K K18, respectively). Note that for K18-V337M, only the fibrils, but not the irregular amorphous structures, were analyzed. Filaments from both K18-WT and K18-N279K were significantly longer than those formed by K18-V337M ( $p < 0.0001$ , Kruskal-Wallis test with Dunn's *post hoc* test; Figure 2D). Filament length between K18-WT and K18-N279K were not significantly different to each other ( $p > 0.9999$ , Kruskal-Wallis test with Dunn's *post hoc* test). However, the three protein variants had significantly different filament widths ( $p < 0.0001$ , Kruskal-Wallis test; mean filament width =  $27.9 \pm 4.2$  nm for K18-WT,  $21.1 \pm 0.8$  nm for



K18-V337M, and  $53.0 \pm 8.3$  nm for K18-N279K), with K18-WT and K18-V337M filaments being similar ( $p = 0.6698$ , Kruskal–Wallis test with Dunn’s *post hoc* test; **Figure 2E**). K18-N279K filaments were significantly wider than those of K18-WT and K18-V337M ( $p < 0.0001$  in both cases, Kruskal–Wallis test with Dunn’s *post hoc* test; **Figure 2E**). Together, the morphology and structural properties of K18-WT aggregates significantly changed in the presence of the FTD mutations, causing a shift from PHFs and SFs to unstructured, amorphous aggregates and shorter but wider filaments for K18-V337M, with K18-N279K aggregating into bundled filaments of similar length to those of K18-WT but of increased width.

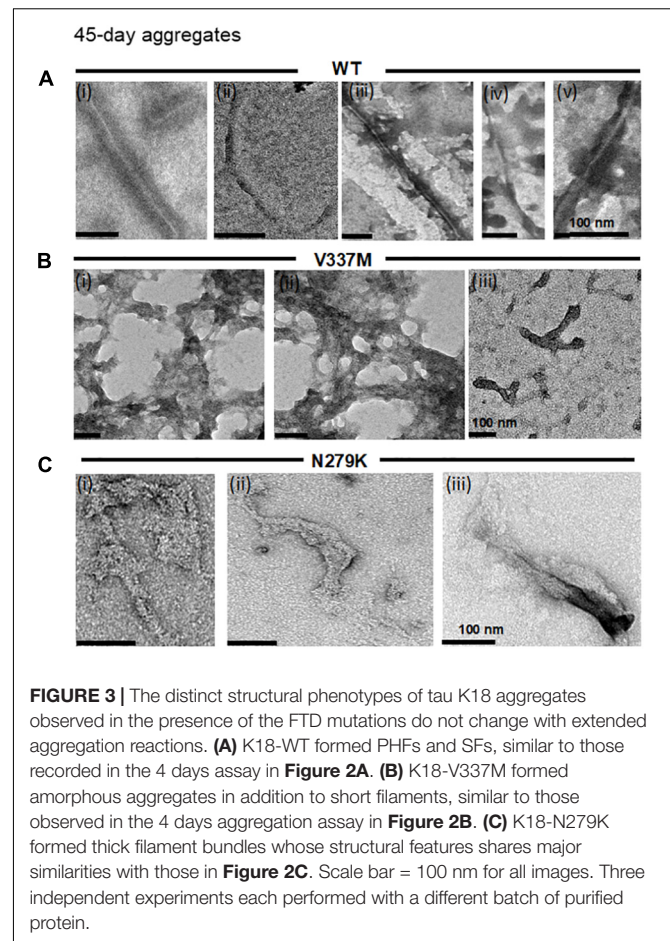
### Phenotypes of Tau K18 Aggregates Do Not Change With Further Incubation

As aggregation and fracture are thought to modulate the aggregation of tau K18 (Meyer et al., 2016), incubation times were increased to ascertain if the structural properties identified after 4 days would be maintained following prolonged incubation. Because aggregate conformation is partly determined by soluble tau recruitment onto template conformers (Margittai and Langen, 2004; Guo and Lee, 2014), it is conceivable that multiple cycles of aggregation and fracture may favor the growth of minor conformers which would otherwise be undetected in shorter experiments (Meyer et al., 2014, 2016). The previously described TEM experimental setup was employed to image samples obtained from extended incubation periods (45 days). The aggregates formed had the same morphological phenotypes as those seen after 4 days for all protein variants (**Figure 3**), indicating that the conformation of K18-WT aggregates is changed by the N279K and V337M mutations, and that these conformations persist during extended incubation.

### FTD Mutations Alter Immuno-Reactivity and Aggregation Products of Tau K18

The unique aggregation and structural properties of the FTD variants of K18 (**Figures 2–3**) are consistent with the hypothesis that they alter K18-WT conformation. In these experiments, heparin was added to accelerate the aggregation and filament formation process. However, the transient nature of heparin-treated tau aggregation can preclude the detection of important conformational changes. The tau proteins’ propensity to self-aggregate into filaments in the heparin-free state and the conformations they adopt during this process were therefore, studied.

Reactivity to specific antibodies (total tau A0024 (K9JA) and T22 oligomer conformation-preferring) was used to test for any further indication of distinct conformations, since proteinopathic protein variants with different conformations can lead have differential immuno-reactivity profiles (Hatami et al., 2017). Incubation time was extended to 314 h without agitation to allow PHF formation. Incipient immuno-reactivity was analyzed by dot blotting (**Figure 4** and **Supplementary Figure S2**). K18-WT had the strongest immuno-reactivity to the total tau antibody

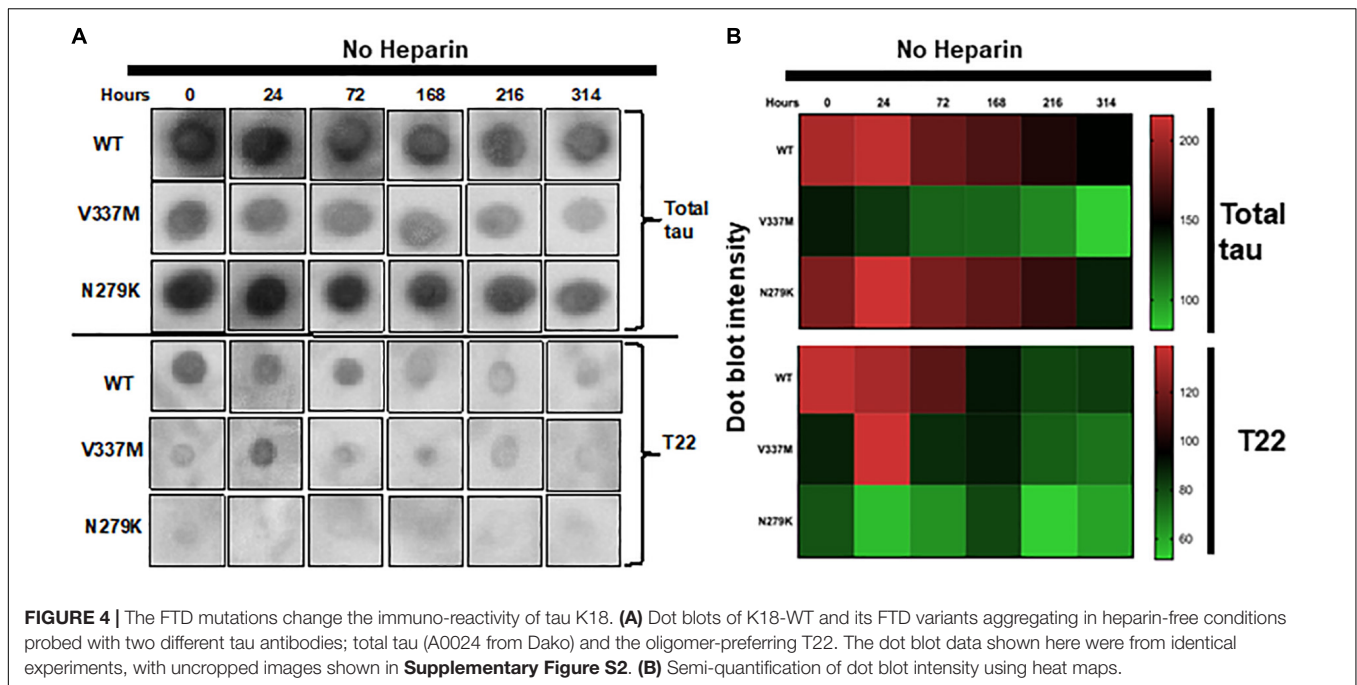


A0024 at 0 h but this decreased over time (**Figures 4A,B**, upper panels). Similar immuno-reactivity, to A0024, of K18-N279K to that of K18-WT was observed, with the highest intensities recorded at early time points. However, K18-V337M had the lowest immuno-reactivity at each time point: the intensity at 0 h, the strongest recorded, was similar to the lowest intensity for K18-WT at 314 h (**Figures 4A,B**).

To gain insight into possible differences in oligomer conformation, reactivity to the oligomer-preferring T22 antibody was analyzed. Similar to its reactivity to A0024, K18-WT had its highest T22 immuno-reactivity at 0 h, which dropped sharply from 168 h onward (**Figures 4A,B**; lower panels). The reactivity of K18-V337M was low at all time points except at 24 h. K18-N279K had the least intensity to T22 at each time point (**Figures 4A,B**; lower panels and **Supplementary Figure S2**). This result implies that each protein variant folds differently with distinct epitope exposure during aggregation.

### Dominant Aggregate Conformers of the Tau K18 Variants Are Unaffected by Seeded Aggregation

Mutations in tau K18 can cause preferential amplification of specific aggregate conformers (Meyer et al., 2014). However, it is unknown if the dominant tau K18 conformers are affected



by seeded aggregation. We therefore, studied if the mutation-induced dominant conformations of the tau K18 variants are affected by the addition of aggregated seeds from different tau K18 variants. Using the same experimental setup as in **Figure 2**, we seeded monomers of tau K18 WT, V337M, and N279K each with 10% volume of 4 days preformed aggregates from each protein variant. Negative-stain TEM imaging showed that seeded reactions (**Supplementary Figures S3B–D**) resulted in aggregate structures with the same phenotypes as those in seed-free experiments (**Supplementary Figure S3A**, same as in **Figure 2**) irrespective of the seed identity. These results suggest that the conformations of the tau K18 aggregates are not only be distinct but may also be incompatible, and that the majority species preferentially aggregate even when seeded with other conformers.

### Preparation and Characterization of Fluorescent K18 Oligomers for Functional Studies

Distinct structures of tau strains are thought to explain their divergent functional effects (Clavaguera et al., 2013; Boluda et al., 2015; Falcon et al., 2015; Narasimhan et al., 2017). We therefore, sought to take advantage of the conformational and aggregation differences of the tau K18 variants to investigate their possible influences on the cellular internalization of exogenously applied oligomers. To achieve this, Alexa Fluor-488-C5-maleimide-labeled oligomers were first prepared as detailed in section “Materials and Methods” and elsewhere (Karikari et al., 2019) before being used in *in vitro* cell culture assays. These stable oligomers were granular and non-fibrillar (**Supplementary Figure S4**).

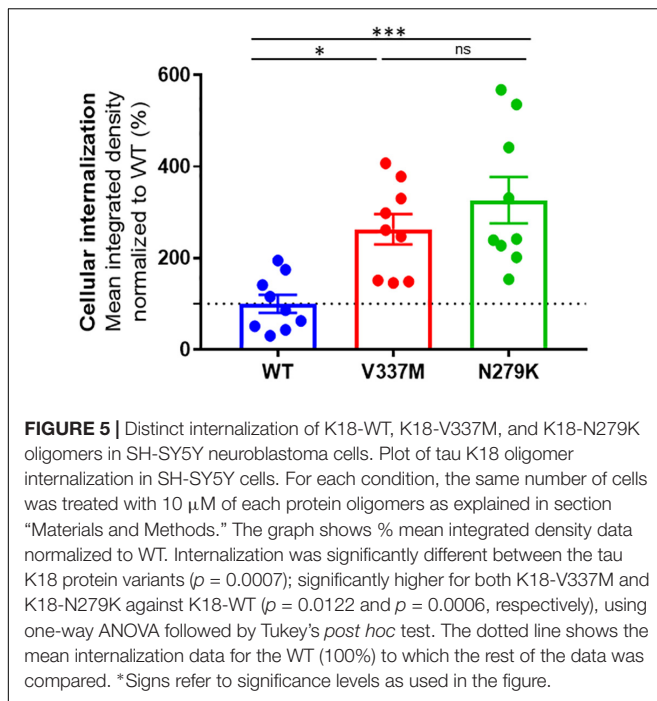
### FTD Mutations Enhance Tau K18 Oligomer Internalization in SH-SY5Y Cells

Increasing evidence suggests that the cellular internalization of tau oligomers is an initial trigger of tau pathology (Usenovic et al., 2015; Kolarova et al., 2017). It is, however, not known if FTD with tau mutations are characterized by the same or similar mechanism. To address this, fluorescently labeled oligomers of K18-WT, K18-V337M, and K18-N279K were applied exogenously to SH-SY5Y cells and their internalization dynamics investigated.

All three tau protein variants were internalized by SH-SY5Y cells (**Supplementary Figures S5–S8**). To account for both diffused and punctate phenotypes, we used integrated density (mean intensity  $\times$  area occupied) to quantify internalized tau in experiments, where equal numbers of cells were seeded and treated with equimolar concentrations of each protein oligomers. The internalization data for each tau K18 variant was analyzed by normalizing the mean integrated density from representative images to the overall mean of the WT (**Figure 5**). Internalization was significantly different between the three protein variants (one-way ANOVA,  $p = 0.0007$ , F statistic = 10.08). The Tukey’s multiple comparison *post hoc* test showed that internalization was significantly higher for both K18-V337M ( $p = 0.0122$ ) and K18-N279K ( $p = 0.0006$ ) against K18-WT but not significantly different between K18-V337M and K18-N279K ( $p = 0.4524$ , **Figure 5**).

### Exogenous Tau K18 Oligomers Are Internalized by Endocytosis

Previous reports have suggested that K18-WT is internalized by endocytosis (Guo and Lee, 2011; Michel et al., 2014).



However, the internalization mechanism of the FTD variants used in this study was not known. The endocytic marker FM4-64<sup>®</sup> (SynaptoRed) was used to stain SH-SY5Y cells during internalization, allowing a preliminary assessment of the localization of the internalized tau. Similar to K18-WT, internalized K18-V337M and K18-N279K oligomers co-localized with FM4-64, suggesting endocytic-dependent internalization (Figures 6A–C). As a control, incubating SH-SY5Y cells seeded with K18 oligomers at 4°C instead of 37°C blocked internalization (Supplementary Figure S9) as shown before for tau K18 and full-length tau 441 (Michel et al., 2014). We next tested if oligomer internalization in a more physiologically relevant cell model, hiPSC-derived neurons, also occurred by endocytosis. Tau taken up by neurons were ostensibly found in both neurites and soma, where they appeared to co-localize with FM4-64 in both compartments (Figures 6D–F). Together, these data suggest that tau K18 oligomers can be internalized by SH-SY5Y cells and hiPSC neurons at least partly through endocytosis.

### Internalized Tau K18 Oligomers Co-localize With Endogenous Tau and the Nuclear Protein Nucleolin

The ability of internalized tau oligomers to interact with endogenous tau is a critical step in the inter-cellular propagation of tau (Lasagna-Reeves et al., 2012a; Michel et al., 2014; Usenovic et al., 2015). It is, however, unknown if tau variants of different conformations will interact with endogenous tau differently upon internalization. Internalized K18 oligomers were observed to co-localize with endogenous tau in hiPSC-derived neurons bearing the <sup>159</sup>PPGQK<sup>163</sup> epitope (HT7 antibody). All three tau K18 variants co-localized with endogenous tau, occurring both in the

neurites and the soma (Figure 7), suggestive of an interaction of internalized tau with endogenous tau.

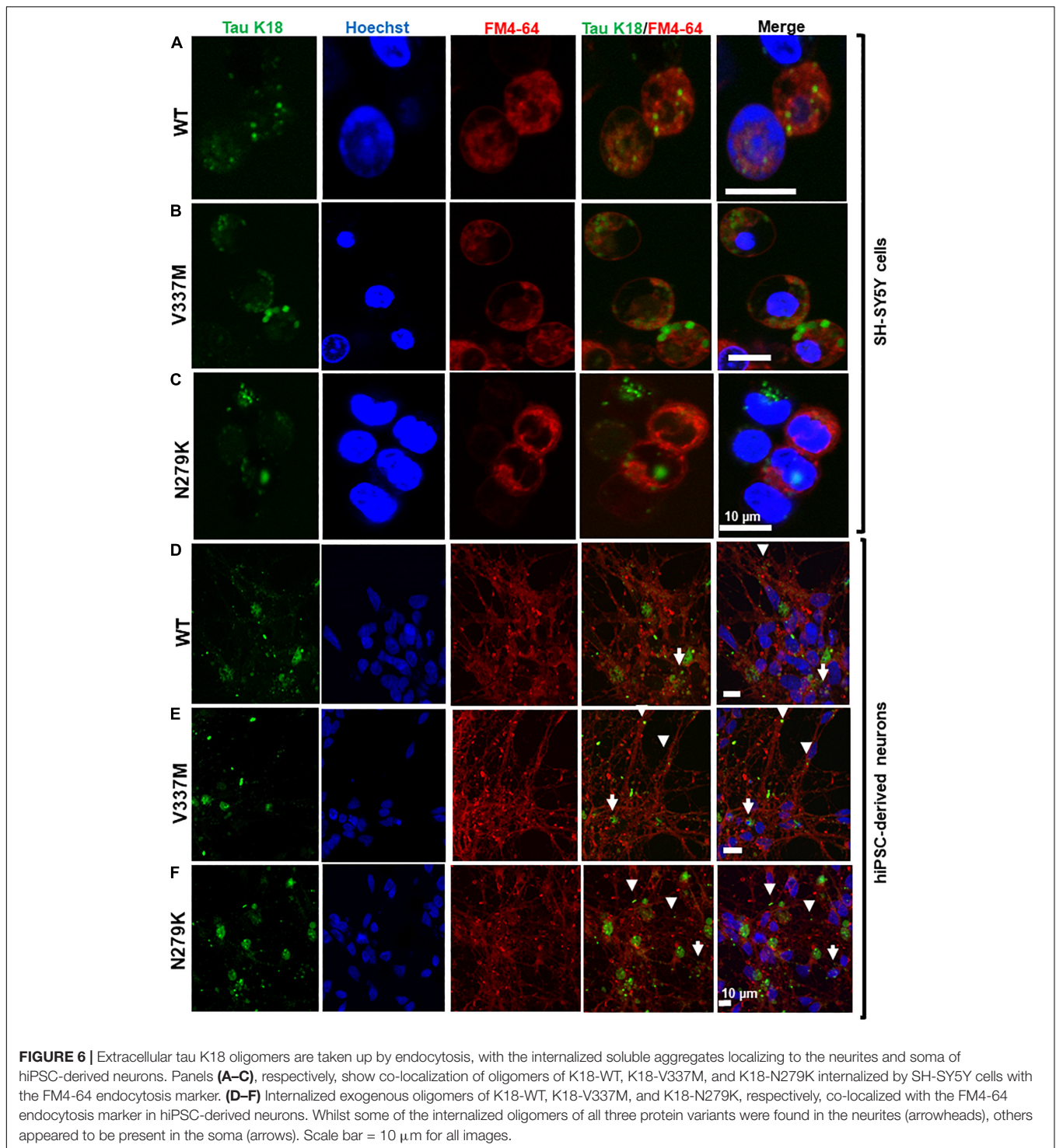
The nuclear localization of both endogenous tau and tau overexpressed from genetic constructs has been reported in both the human and mouse brains (Rady et al., 1995; Liu and Götz, 2013) and cell culture models (Lu et al., 2014; Ritter et al., 2018). Nuclear tau staining is often predominantly apparent in the nucleolus, with tau signals co-localized with those of the nucleolar protein nucleolin (Sjöberg et al., 2006), although more diffuse nuclear staining for endogenous tau has been reported in response to cell stress (Sultan et al., 2011). In SH-SY5Y cells, the internalized tau was not generally detected in the nucleus. Although some association with nucleolin was observed, this was expected to result from the redistribution of the nucleolin protein during the different phases of the cell cycle in these dividing cells (data not shown). Cytoplasmic accumulation of internalized tau, as has been previously demonstrated, was recorded for both cell types. However, in contrast to the SH-SY5Y cells, tau-nucleolin co-localization was observed in hiPSC-derived neurons with nucleolar inclusion of internalized tau for both mutant and WT tau-K18 (Figure 8).

### Internalized Tau K18 Oligomers Do Not Induce LDH-Dependent Cytotoxicity in SH-SY5Y Cells

Several studies have shown that internalized tau oligomers impair cell viability and/or induce cell death (Lasagna-Reeves et al., 2010; Guerrero-Muñoz et al., 2015) but others have reported the opposite (Kumar et al., 2014; Kaniyappan et al., 2017). However, the cytotoxicity potential of tau FTD variants is unknown. SH-SY5Y cells were therefore, treated with the respective oligomers and cytotoxicity studied by measuring LDH release. No significant differences in viability were observed between increasing concentrations of WT or mutant K18 oligomers (Figure 9), suggesting that the oligomers did not induce LDH-dependent cytotoxicity over 72 h.

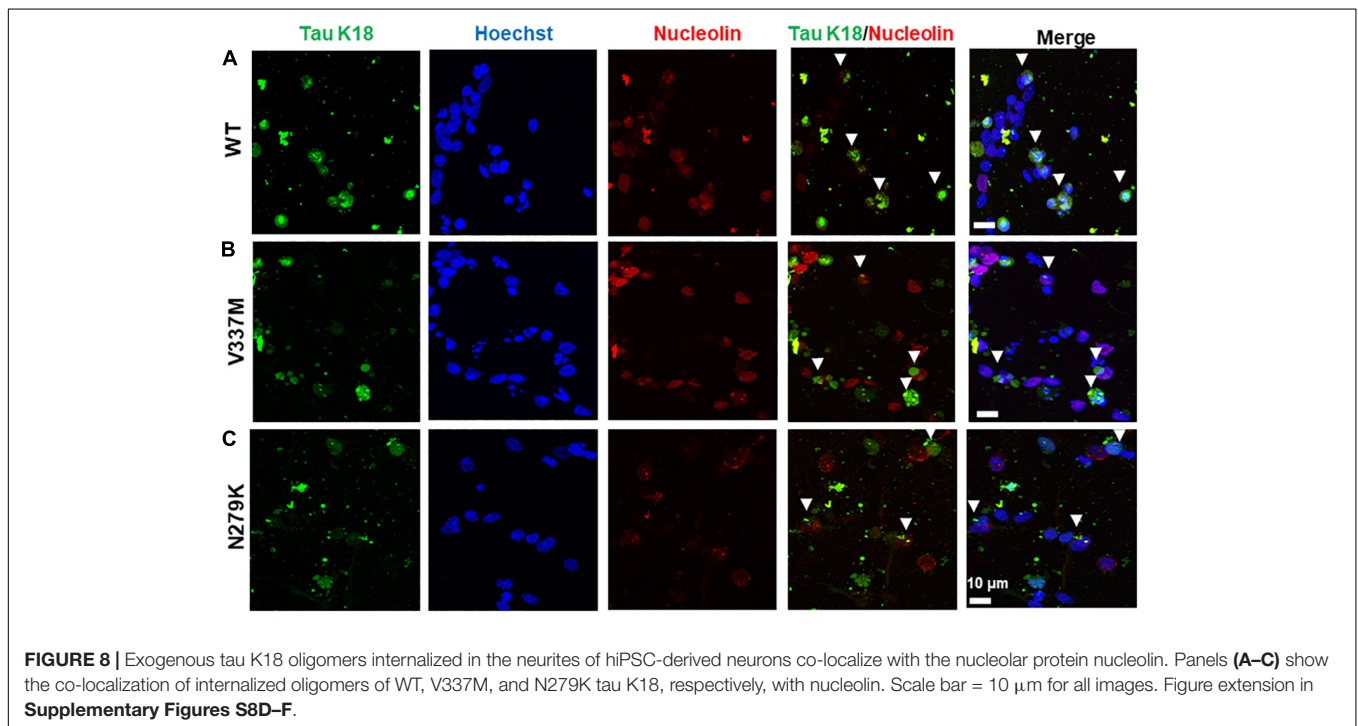
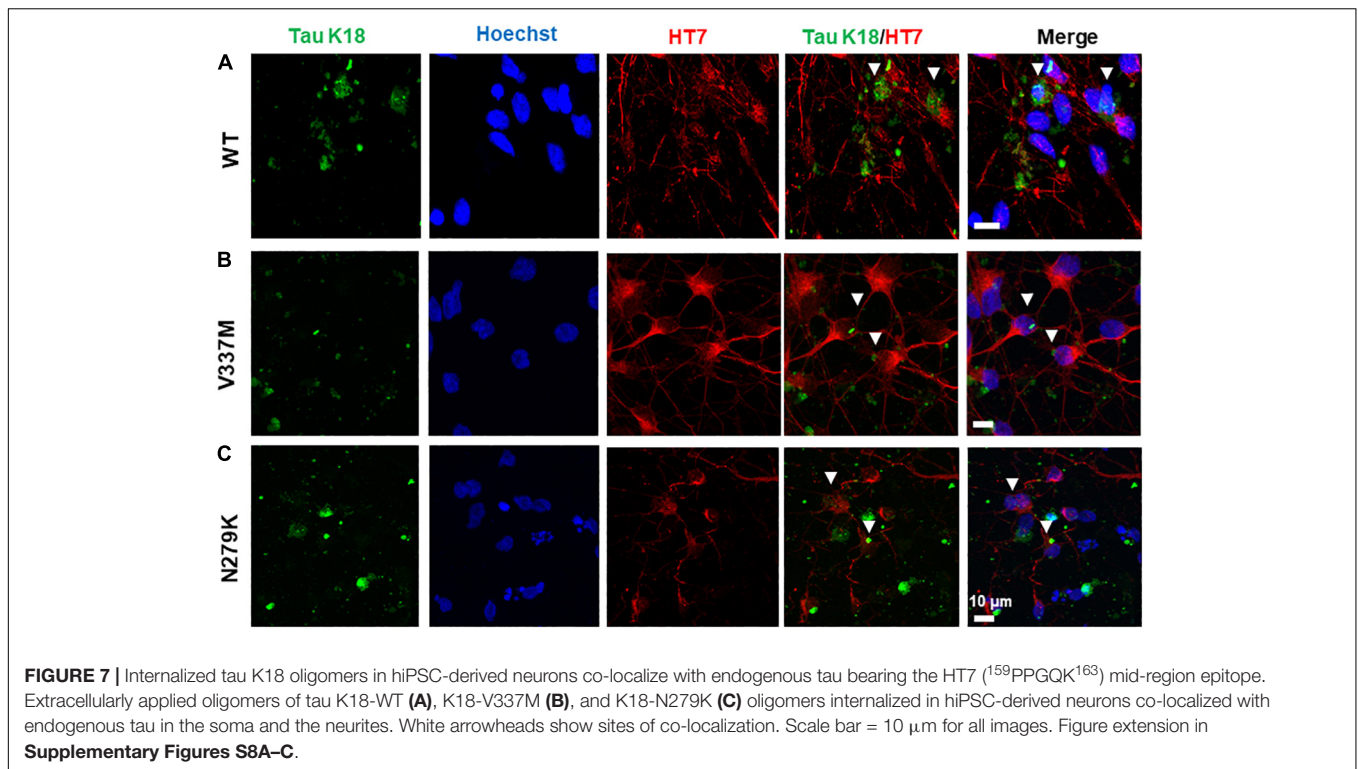
## DISCUSSION

Tau has important functions in the pathogenesis of AD and FTD (Ghetti et al., 2015; Wang and Mandelkow, 2016; Guo et al., 2017). Whilst several theories have been proposed toward understanding disease mechanisms, recent studies have pointed to possible involvement of an inter-neuronal transmission mechanism. Although this hypothesis has strong evidential support (Mohamed et al., 2013; Guo and Lee, 2014; Hu et al., 2016), it remains to be shown why tau isolates from different post-mortem tauopathy brains have distinct internalization and transmission capabilities. In this study, an integrated structural and cell biological approach was used to understand potential links between protein aggregation, conformation and cellular internalization. It was hypothesized that specific disease-associated *MAPT* mutations implicated in familial FTD will alter the structural features (conformation and aggregation) and cellular internalization of WT tau K18. It has been demonstrated that the N279K and V337M FTD-linked mutations do alter



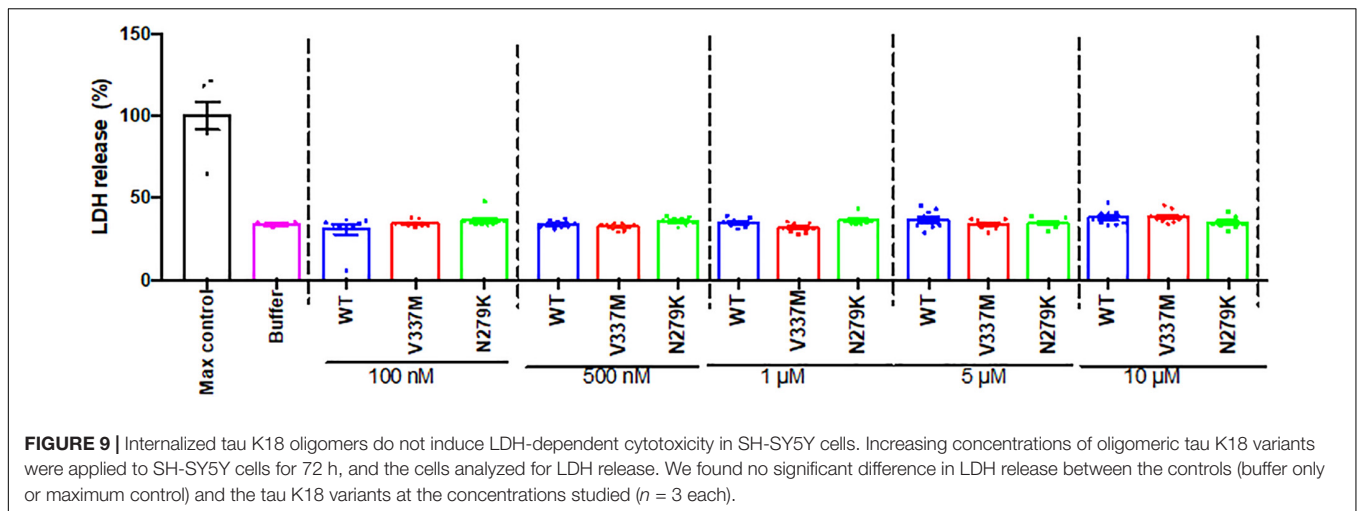
tau K18 aggregation and conformation. Moreover, the mutants had enhanced cellular internalization, yet all protein variants were internalized by endocytosis and had shared the same sub-cellular accumulation patterns. These data suggest that structural distinctions between tau variants may influence their cellular internalization properties, with potential implications for the molecular pathogenesis of tauopathies.

Previous studies of the V337M and N279K mutations did not identify any discernible effects on tau aggregation propensity (Barghorn et al., 2000; Combs and Gamblin, 2012). This may have been due to the use of thioflavin fluorescent reporter assays to quantify aggregation (Barghorn et al., 2000; Combs and Gamblin, 2012). Although commonly used to detect cross β-sheet-dependent aggregation (Lindberg et al., 2015), a major



pitfall of thioflavin assays is that they appear to be probes of protein conformation instead of aggregation status since different folding behaviors can change the availability of different proteinopathic proteins to the binding sites of the dye (Coelho-Cerqueira et al., 2014; Wong et al., 2016; Hatami et al., 2017).

For this reason, the ability of thioflavin dyes to distinguish between conformations of variants of the same protein can sometimes be complicated (Hatami et al., 2017). Although kinetics may remain apparently unaffected, our data using TEM to characterize aggregates suggest that both mutations



impact upon the aggregation of K18, a finding supported by atomic force microscopy analysis (data not shown). Immunoreactivity data to probe conformation supported these findings. These complementary findings in multiple assays build a strong argument in support of the hypothesis that the mutations alter the aggregation and conformation of tau K18. Interestingly, similar profiles were observed for aggregation reactions carried out in the absence of the heparin aggregation inducer. Moreover, the FTD mutations altered the immuno-reactivity of aggregated K18-WT. K18-V337M had lower reactivity to both tau antibodies whilst the N279K mutation almost abolished reactivity to the oligomer-preferring T22 antibody but its reactivity to A0024 was comparable to that of K18-WT. Our results therefore, imply that each mutation shifts protein conformation which in turn dictates the pathway toward forming distinct aggregates. The consistent observation that each protein variant had distinct aggregate structures in several independent assays (both heparin-induced and native-state aggregation) additionally supports mutation-induced differences in protein aggregation and conformations, similar to that previously described for amyloid beta (Hatami et al., 2017). Two main reasons could account for the distinct T22 reactivity even at 0 h, where the samples were monomeric. Firstly, the T22 antibody is thought to selectively recognize an oligomeric conformational epitope. However, the antibody can also react with monomers which presumably share this same epitope (Lasagna-Reeves et al., 2012b). Secondly, the differential T22 binding to the tau K18 variants could also be due to the introduced mutations since the exact epitope of the antibody is unknown (it binds to the repeat domain region – amino acids 244–372 of full length tau 441). It is conceivable that the distinct aggregation and conformational dynamics of the protein variants would also lead to notable differences in epitope availability/recognition. Together, the data provided demonstrate that the V337M and N279K disease-associated mutations induce structural and conformational changes in tau K18 that are evident at distinct stages of aggregation, including oligomers and fibrils.

Tau oligomers are a potential sensitive biomarker for neurodegeneration (Sengupta et al., 2017) and can induce

endogenous tau aggregation upon cellular internalization (Lasagna-Reeves et al., 2012a; Michel et al., 2014). Effects of the disease mutations on the cellular uptake of structurally characterized oligomers of tau K18 were therefore investigated. Differences in oligomer uptake were observed in respect to tau mutants. Irrespective of mutation, the uptake of K18 appeared to be endocytic. Uptake of all K18 forms tested highlight that different tau aggregates may each propagate disease by spreading into non-diseased cells. However, differences potentially mediated by aggregate conformation may provide critical insights into shared and distinct molecular mechanisms of tauopathies involving FTD and WT tau.

Consistent with previous reports that used recombinant or brain isolates of tau (Frost et al., 2009; Guo and Lee, 2011; Michel et al., 2014; Falcon et al., 2015; Ando et al., 2016; Calafate et al., 2016), the K18-WT oligomers were most likely internalized by endocytosis in both cell types, with same observed for the FTD variants. Whilst all protein variants appeared to be internalized by endocytosis, co-localized with endogenous tau and were found both in the cytoplasm and nucleus, the degree of internalization differed between the protein variants. We speculative that the new aggregation and/or conformation dynamics recorded in the presence of the FTD mutations may change tau K18 interaction with cell surface proteins that regulate endocytosis, resulting in altered cellular trafficking. In agreement, binding to heparan sulfate proteoglycans regulates the cellular internalization and inter-cellular propagation of aggregated tau, and that blocking the activity or expression of heparan sulfate proteoglycan prevents internalization (Holmes et al., 2013; Rauch et al., 2018). However, it is unknown if WT and mutant tau proteins bind heparan sulfate proteoglycans with the same or different affinities. Furthermore, dysfunctions in key steps in clathrin-mediated endocytosis have been implicated in tau propagation and inclusion formation in AD, FTD and other tauopathies (Ando et al., 2016; Calafate et al., 2016). It remains to be studied if mutation-induced conformational changes do modify tau internalization, propagation and toxicity in an *in vivo* model. However, with the *in vitro* evidence presented in the

current study, we can speculate that the altered conformations of tau resulting from the FTD mutations leads to specific changes in the protein's vesicular uptake or receptor binding, resulting in altered uptake efficiency. Another possibility is that the FTD mutations alter the efficiency of degradation of internalized tau K18 in each cell line, resulting in differential amounts of internalized proteins. It is worth investigating if oligomers of WT and mutated tau are degraded through the same or different pathways, and if the mutations affect clearance efficiency. Previous studies have shown that internalized WT tau oligomers/aggregates and the internalized-endogenous tau aggregate complexes they form intracellularly may be cleared by autophagy (Wu et al., 2013; Usenovic et al., 2015). In agreement, treating hiPSC-derived neurons with rapamycin reduces the amount of internalized tau oligomers-endogenous tau aggregate complexes, suggesting that lysosomal elimination is a common degradation route for tau aggregates.

The ability of internalized exogenous tau aggregates to interact with endogenous tau is critical for the efficient inter-cellular propagation of tau aggregates and the associated neurotoxicity (Lasagna-Reeves et al., 2012a; Michel et al., 2014; Wegmann et al., 2015). The observed co-localization of all three protein variants with endogenous tau suggests that internalized tau K18 and the FTD variants can interact with endogenous tau, indicating the potential for propagation by inducing endogenous tau aggregation, possibly following a templated misfolding mechanism as described previously for tau K18 (Guo and Lee, 2011; Michel et al., 2014). As both the FTD mutants and WT K18 showed similar cellular distribution and localization, it would suggest the potential for prion-like propagation of the FTD mutant tau.

In hiPSC-derived neurons, the co-localization with nucleolin suggests that internalized tau can be taken up into the nucleus, and raises the possibility that internalized tau that gets into the nucleus may have functions in protein biosynthesis. Nuclear tau associates with nucleolin in AD brain, where reduced nuclear tau levels correlated with decreased amounts of nucleolin (Hernández-Ortega et al., 2016). Interaction of aggregated tau, both WT and disease-associated mutated variants, with specific ribosomal proteins can impair the protein synthesis machinery (Meier et al., 2016). Given that pathological tau can impair nucleocytoplasmic transport in AD brains and tau transgenic mice (Eftekharzadeh et al., 2018), and the overexpression of the N279K tau variant in a cell model is associated with increased nuclear localization (Ritter et al., 2018), the effect of tau on the protein synthesis machinery deserves further investigation.

Our findings that tau K18 oligomers, even at high concentrations, did not significantly induce LDH release was unexpected since some previous reports pointed to the contrary (Lasagna-Reeves et al., 2010, 2012a). Nonetheless, our present data is supported by other studies (Kumar et al., 2014; Tepper et al., 2014; Kaniyappan et al., 2017). The origin of these divergent data is unknown but could be explained by differences in oligomer concentrations, preparation methods and cytotoxicity assays. For example, 0.1–1  $\mu$ M of full length tau-441 oligomers produced by seeding with oligomers from AD brain, amyloid  $\beta$  or  $\alpha$ -synuclein were toxic to cells, as measured by

the 3-(4,5-dimethylthiazol-2-yl)-5-(3-carboxymethoxyphenyl)-2-(4-sulfophenyl)-2H-tetrazolium (MTS) assay (Lasagna-Reeves et al., 2010, 2012a). On the other hand, applying 10  $\mu$ M of tau K18 oligomers (recombinant or derived from Sf9 cells) to mouse primary cortical neurons or SH-SY5Y cells did not result in significant cytotoxicity within 3–72 h, as shown by the LDH or MTT (3-(4,5-dimethylthiazol-2-yl)-2,5-diphenyltetrazolium bromide) assays (Kumar et al., 2014; Tepper et al., 2014). Whether or not exogenous tau oligomers induce overt cytotoxicity, their most immediate toxic effect is likely to be an impairment of the structural and functional integrity of neurons and potentially other cell types. In support, internalized tau oligomers impair neural transmission, cause dendritic spine loss and increases in intracellular calcium levels and reactive oxygen species without evidence of overt changes to cell viability (Kumar et al., 2014; Tepper et al., 2014; Usenovic et al., 2015; Yin et al., 2016; Kaniyappan et al., 2017).

Together, these results demonstrate that specific disease-associated single nucleotide polymorphisms in tau can cause drastic changes in protein conformation and aggregation. These distinctive structural and conformational properties may be crucial determinants of the inter-cellular transmission efficiency of the oligomeric forms of these proteins. These findings may provide a molecular explanation as to why tau extracts obtained from different sources (including human tauopathy brains, tau transgenic mice brains, and recombinant preparations) have distinctive propagation potencies and endogenous tau aggregation abilities in both cellular and animal preclinical tauopathy models. Indeed, aggregated tau from transgenic mice brains and recombinant sources have been shown to have distinct conformations that can influence their seeding capabilities (Falcon et al., 2015). It can be argued that critical post-translational modifications such as phosphorylation and the *in vivo* environment in which this process occurs might have contributed to the conformational differences observed. As the recombinant tau proteins used in the present study were not phosphorylated, it can be said that phosphorylation and sites of phosphorylation *per se* may not be responsible for the conformational, structural and molecular activity differences previously observed for tau aggregates from diverse sources. The differential aggregation of the recombinant mutants reinforces the conclusion that specific amino acid modifications are sufficient to induce structural and functional differences in tau-K18. Such structural and functional differences may then be compounded by the differential phosphorylation of the mutant forms of tau or their differential recruitment of endogenous tau.

Importantly, these findings may help to understand why different tauopathies have distinct progression rates, neuropathological features, inclusion formation and types of inclusion (Delisle et al., 1999; Murrell et al., 1999; Sergeant et al., 2005; Ghetti et al., 2015). Furthermore, these results may pave the way for the development of more sensitive, disease- and mutation-specific platforms for early, more accurate diagnosis of tauopathies. Future studies should aim to ascertain if the findings described here are applicable to tau isolates from tauopathy brains: if their reported activity differences can be explained by structural and conformational distinctions.

## AUTHOR CONTRIBUTIONS

TK, DN, EH, and KM conceived and co-ordinated the study. TK designed and conducted the experiments, analyzed the data, and wrote the first draft of the manuscript. AG, CC-B, and JC made significant contributions to hiPSC experiments, immunocytochemistry, and confocal microscopy. DN, EH, and KM contributed reagents and materials, made important contributions to data interpretation, and critically revised the initial manuscript draft. All authors discussed and commented on the final manuscript.

## FUNDING

The authors acknowledge support from the CRACK IT: Untangle grant (NC/C013101/1) awarded by the National Centre for the Replacement, Refinement and Reduction of Animals in Research. TK was funded by a joint studentship from the University of Warwick Chancellor's Scholarship and the Biotechnology and Biological Sciences Research Council (BBSRC) grant number BB/J014532/1, through the Midlands Integrative Biosciences Training Partnership. The funders had no role in study design, data collection and analysis, decision to publish, or preparation of the manuscript.

## ACKNOWLEDGMENTS

The authors wish to thank Prof. Alison Rodger and Dr. Nikola Chmel of the Department of Chemistry, University of Warwick, for useful discussions and use of analytical biophysics facilities. The authors also thank Mr. Ian Hands-Portman (School of Life Sciences, University of Warwick) for training TK and providing him access to TEM facilities. TK acknowledges Drs. Mussa Quareshy and Greg Walkowiak for assistance with protein purification and microplate reader access, respectively. The authors acknowledge support from the Research Councils UK Block Grant at the University of Warwick for the payment of open access fee.

## SUPPLEMENTARY MATERIAL

The Supplementary Material for this article can be found online at: <https://www.frontiersin.org/articles/10.3389/fncel.2019.00296/full#supplementary-material>

**FIGURE S1** | The FTD mutations cause structural changes in the properties of tau K18 filaments. **(A)** Representative TEM images of K18-WT, showing PHFs and

SFs. **(B)** Representative electron micrographs of K18-V337M, which formed amorphous aggregates [examples shown in (i), (ii), and (iii)] and short filaments [(iv) and (v)]. **(C)** Representative electron micrographs of K18-N279K, showing bundled filaments of varying shapes and widths. Scale bar = 100 nm for all images.  $n = 3$  independent experiments for each protein. This figure is an extension of **Figure 2**.

**FIGURE S2** | Uncropped dot blot data used for immuno-reactivity analysis in **Figure 4**. **(A)** Dot blot intensity data for K18-WT, K18-V337M, and K18-N279K following total tau A0024 reactivity. **(B)** T22 antibody reactivity profiles of K18-WT, K18-V337M, and K18-N279K. For better visualization, the sites of dot blotting are highlighted with black circles.

**FIGURE S3** | Dominant aggregate conformers of the tau K18 variants are unaffected by seeded aggregation. Endpoint aggregates of K18 WT, V337M, and N279K from 4 days reactions were used to seed the aggregation of each protein in turn. The resulting product, after a further 4 days of incubation at room temperature, were analyzed by TEM imaging **(A)**, unseeded; **(B)**, seeded with WT; **(C)**, seeded with V337M seeded; and **(D)**, seeded with N279K. Scale bars = 100 nm for all images.

**FIGURE S4** | Structural characterization of fluorescently labeled oligomers of tau K18 and its FTD variants. **(A–C)** Representative TEM characterization of tau K18 oligomers labeled with Alexa Fluor 488 conjugated maleimide demonstrating the presence of granular structures for K18-WT, K18-V337M, and K18-N279K, respectively. Insets refer to higher magnification images. Scale bars for all images = 200 nm and 20 nm for insets. **(D)** Non-denaturing SDS PAGE image of labeled tau K18 oligomers.

**FIGURE S5** | Uptake of extracellularly applied tau K18 oligomers into SH-SY5Y cells. Seeded cells were supplied with 10  $\mu$ M tau K18 oligomers and incubated for 24 h at 37°C, 5% CO<sub>2</sub>, following which the spent media were removed and the cells washed with warm 10 mM PBS before new tau-free media was added. Uptake of oligomers was demonstrated using confocal microscopy. Panels **(A–C)** show cellular internalization of K18-WT, K18-V337M, and K18-N279K oligomers, respectively. Scale bar = 10  $\mu$ m for all images.

**FIGURE S6** | Internalized oligomers of the tau K18 variants localize to the nuclei and cytoplasm of SH-SY5Y cells. Oligomeric aggregates of tau K18-WT **(A)**, K18-V337M **(B)**, and K18-N279K **(C)** internalized by the SH-SY5Y cells appeared to be distributed in the cytoplasm (open arrow heads) and nucleus (filled arrow heads). Scale bars = 10  $\mu$ m for all images.

**FIGURE S7** | Higher resolution images of internalized tau K18 oligomers in SH-SY5Y cells. The images here show AF-maleimide-labeled tau K18 oligomers (green) taken up mainly into the cytoplasm of K18-WT, K18-V337M, and K18-N279K **(A–C)**, respectively. Scale bar = 10  $\mu$ m for all images.

**FIGURE S8** | Colocalization of tau K18 with endogenous tau and nucleolin at high intensity. These figures show digitally increased intensity of selected regions from the images in **Figures 7, 8** to better demonstrate colocalization of tau K18 WT, V337M, and N279K with endogenous tau **(A–C)**, respectively) or nucleolin **(D–F)**, respectively). For better composite color appreciation, colocalization is shown in yellow - merger of red (endogenous tau or nucleolin) and green (tau K18) channels or white - merger of magenta (endogenous tau or nucleolin) and green (tau K18) channels. Arrows point to regions of colocalization.

**FIGURE S9** | Incubation in cold conditions blocks the internalization of tau K18 oligomers by SH-SY5Y cells. **(A–C)** Oligomer uptake was significantly reduced for tau K18-WT, K18-V337M, and K18-N279K, respectively when SH-SY5Y cells were incubated at 4°C instead of 37°C (as shown in **Figure 6**).

## REFERENCES

- Alonso, A. D., Beharry, C., Corbo, C. P., and Cohen, L. S. (2016). Molecular mechanism of prion-like tau-induced neurodegeneration. *Alzheimers Dement.* 12, 1090–1097. doi: 10.1016/j.jalz.2015.12.014
- Ando, K., Tomimura, K., Sazdovitch, V., Suain, V., Yilmaz, Z., Authalet, M., et al. (2016). Level of PICALM, a key component of clathrin-mediated endocytosis, is correlated with levels of phosphotau and autophagy-related proteins and is associated with tau inclusions in AD, PSP and Pick disease. *Neurobiol. Dis.* 94, 32–43. doi: 10.1016/j.nbd.2016.05.017
- Arriagada, P. V., Growdon, J. H., Hedley-Whyte, E. T., and Hyman, B. T. (1992). Neurofibrillary tangles but not senile plaques parallel duration and severity of Alzheimer's disease. *Neurology* 42, 631–639.

- Barghorn, S., Davies, P., and Mandelkow, E. (2004). Tau paired helical filaments from Alzheimer's Disease brain and assembled in vitro are based on  $\beta$ -structure in the core domain. *Biochemistry* 43, 1694–1703. doi: 10.1021/bi0357006
- Barghorn, S., and Mandelkow, E. (2002). Toward a unified scheme for the aggregation of tau into Alzheimer paired helical filaments†. *Biochemistry* 41, 14885–14896. doi: 10.1021/bi026469j
- Barghorn, S., Zheng-Fischhöfer, Q., Ackmann, M., Biernat, J., von Bergen, M., Mandelkow, E.-M., et al. (2000). Structure, microtubule interactions, and paired helical filament aggregation by tau mutants of frontotemporal dementias. *Biochemistry* 39, 11714–11721. doi: 10.1021/bi000850r
- Bodea, L., Eckert, A., Ittner, L. M., Piguet, O., and Götz, J. (2016). Tau physiology and pathomechanisms in frontotemporal lobar degeneration. *J. Neurochem.* 138, 71–94. doi: 10.1111/jnc.13600
- Boluda, S., Iba, M., Zhang, B., Raible, K. M., Lee, V. M.-Y., and Trojanowski, J. Q. (2015). Differential induction and spread of tau pathology in young PS19 tau transgenic mice following intracerebral injections of pathological tau from Alzheimer's disease or corticobasal degeneration brains. *Acta Neuropathol.* 129, 221–237. doi: 10.1007/s00401-014-1373-1370
- Calafate, S., Flavin, W., Verstreken, P., and Moechars, D. (2016). Loss of bin1 promotes the propagation of tau pathology. *Cell Rep.* 17, 931–940. doi: 10.1016/j.celrep.2016.09.063
- Clavaguera, F., Akatsu, H., Fraser, G., Crowther, R. A., Frank, S., Hench, J., et al. (2013). Brain homogenates from human tauopathies induce tau inclusions in mouse brain. *Proc. Natl. Acad. Sci. U.S.A.* 110, 9535–9540. doi: 10.1073/pnas.1301175110
- Clavaguera, F., Bolmont, T., Crowther, R. A., Abramowski, D., Frank, S., Probst, A., et al. (2009). Transmission and spreading of tauopathy in transgenic mouse brain. *Nat. Cell Biol.* 11, 909–913. doi: 10.1038/ncb1901
- Coelho-Cerqueira, E., Pinheiro, A. S., and Follmer, C. (2014). Pitfalls associated with the use of Thioflavin-T to monitor anti-fibrillogenic activity. *Bioorg. Med. Chem. Lett.* 24, 3194–3198. doi: 10.1016/j.bmcl.2014.04.072
- Combs, B., and Gambin, T. C. (2012). FTDP-17 tau mutations induce distinct effects on aggregation and microtubule interactions. *Biochemistry* 51, 8597–8607. doi: 10.1021/bi3010818
- Delisle, M. B., Murrell, J. R., Richardson, R., Trofatter, J. A., Rascol, O., Soulages, X., et al. (1999). A mutation at codon 279 (N279K) in exon 10 of the Tau gene causes a tauopathy with dementia and supranuclear palsy. *Acta Neuropathol.* 98, 62–77. doi: 10.1007/s0040100051052
- Eftekharzadeh, B., Daigle, J. G., Kapinos, L. E., Coyne, A., Schiantarelli, J., Carlomagno, Y., et al. (2018). Tau protein disrupts nucleocytoplasmic transport in Alzheimer's Disease. *Neuron* 99, 925–940.e7. doi: 10.1016/j.neuron.2018.07.039
- Falcon, B., Cavallini, A., Angers, R., Glover, S., Murray, T. K., Barnham, L., et al. (2015). Conformation Determines the seeding potencies of native and recombinant tau aggregates. *J. Biol. Chem.* 290, 1049–1065. doi: 10.1074/jbc.M114.589309
- Fitzpatrick, A. W. P., Falcon, B., He, S., Murzin, A. G., Murshudov, G., Garringer, H. J., et al. (2017). Cryo-EM structures of tau filaments from Alzheimer's disease. *Nature* 547, 185–190. doi: 10.1038/nature23002
- Frost, B., Jacks, R. L., and Diamond, M. I. (2009). Propagation of tau misfolding from the outside to the inside of a cell. *J. Biol. Chem.* 284, 12845–12852. doi: 10.1074/jbc.M808759200
- Gerson, J. E., Mudher, A., and Kaye, R. (2016). Potential mechanisms and implications for the formation of tau oligomeric strains. *Crit. Rev. Biochem. Mol. Biol.* 51, 482–496. doi: 10.1080/10409238.2016.1226251
- Ghetti, B., Oblak, A. L., Bovee, B. F., Johnson, K. A., Dickerson, B. C., and Goedert, M. (2015). Frontotemporal dementia caused by microtubule-associated protein tau gene (MAPT) mutations: a chameleon for neuropathology and neuroimaging. *Neuropathol. Appl. Neurobiol.* 41, 24–46. doi: 10.1111/nan.12213
- Goedert, M. (2016). The ordered assembly of tau is the gain-of-toxic function that causes human tauopathies. *Alzheimers Dement.* 12, 1040–1050. doi: 10.1016/j.jalz.2016.09.001
- Goedert, M., Falcon, B., Clavaguera, F., and Tolnay, M. (2014). Prion-like Mechanisms in the Pathogenesis of Tauopathies and Synucleinopathies. *Curr. Neurol. Neurosci. Rep.* 14:495. doi: 10.1007/s11910-014-0495-z
- Grüning, C. S. R., Mirecka, E. A., Klein, A. N., Mandelkow, E., Willbold, D., Marino, S. F., et al. (2014). Alternative conformations of the tau repeat domain in complex with an engineered binding protein. *J. Biol. Chem.* 289, 23209–23218. doi: 10.1074/jbc.M114.560920
- Guerrero-Muñoz, M. J., Gerson, J., and Castillo-Carranza, D. L. (2015). Tau oligomers: the toxic player at synapses in Alzheimer's Disease. *Front. Cell. Neurosci.* 9:464. doi: 10.3389/fncel.2015.00464
- Guo, J. L., and Lee, V. M. (2014). Cell-to-cell transmission of pathogenic proteins in neurodegenerative diseases. *Nat. Med.* 20, 130–138. doi: 10.1038/nm.3457
- Guo, J. L., and Lee, V. M.-Y. (2011). Seeding of normal Tau by pathological Tau conformers drives pathogenesis of Alzheimer-like tangles. *J. Biol. Chem.* 286, 15317–15331. doi: 10.1074/jbc.M110.209296
- Guo, T., Noble, W., and Hanger, D. P. (2017). Roles of tau protein in health and disease. *Acta Neuropathol.* 133, 665–704. doi: 10.1007/s00401-017-1707-1709
- Hatami, A., Monjazeb, S., Milton, S., and Glabe, C. G. (2017). Familial Alzheimer's Disease Mutations within the Amyloid Precursor Protein Alter the Aggregation and Conformation of the Amyloid- $\beta$  Peptide. *J. Biol. Chem.* 292, 3172–3185. doi: 10.1074/jbc.M116.755264
- Hernández-Ortega, K., García-Esparcia, P., Gil, L., Lucas, J. J., and Ferrer, I. (2016). Altered machinery of protein synthesis in Alzheimer's: from the nucleolus to the ribosome. *Brain Pathol.* 26, 593–605. doi: 10.1111/bpa.12335
- Holmes, B. B., DeVos, S. L., Kfoury, N., Li, M., Jacks, R., Yamamandra, K., et al. (2013). Heparan sulfate proteoglycans mediate internalization and propagation of specific proteopathic seeds. *Proc. Natl. Acad. Sci.* 110, E3138–E3147. doi: 10.1073/pnas.1301440110
- Hong, M., Zhukareva, V., Vogelsberg-Ragaglia, V., Wszolek, Z., Reed, L., Miller, B. I., et al. (1998). Mutation-specific functional impairments in distinct tau isoforms of hereditary FTDP-17. *Science* 282, 1914–1917. doi: 10.1126/science.282.5395.1914
- Hu, W., Zhang, X., Tung, Y. C., Xie, S., Liu, F., and Iqbal, K. (2016). Hyperphosphorylation determines both the spread and the morphology of tau pathology. *Alzheimers Dement.* 12, 1066–1077. doi: 10.1016/j.jalz.2016.01.014
- Iba, M., Guo, J. L., McBride, J. D., Zhang, B., Trojanowski, J. Q., and Lee, V. M.-Y. (2013). Synthetic Tau Fibrils Mediate Transmission of Neurofibrillary Tangles in a Transgenic Mouse Model of Alzheimer's-Like Tauopathy. *J. Neurosci.* 33, 1024–1037. doi: 10.1523/JNEUROSCI.2642-12.2013
- Kaniyappan, S., Chandupatla, R. R., Mandelkow, E.-M., and Mandelkow, E. (2017). Extracellular low-n oligomers of tau cause selective synaptotoxicity without affecting cell viability. *Alzheimers Dement.* 13, 1270–1291. doi: 10.1016/j.jalz.2017.04.002
- Karikari, T. K., Nagel, D. A., Grainger, A., Clarke-Bland, C., Hill, E. J., and Moffat, K. G. (2019). Preparation of stable tau oligomers for cellular and biochemical studies. *Anal. Biochem.* 566, 67–74. doi: 10.1016/j.ab.2018.10.013
- Karikari, T. K., Turner, A., Stass, R., Lee, L. C. Y., Wilson, B., Nagel, D. A., et al. (2017). Expression and purification of tau protein and its frontotemporal dementia variants using a cleavable histidine tag. *Protein Expr. Purif.* 130, 44–54. doi: 10.1016/j.pep.2016.09.009
- Kaufman, S. K., Sanders, D. W., Thomas, T. L., Ruchinskas, A. J., Vaquer-Alicea, J., Sharma, A. M., et al. (2016). Tau prion strains dictate patterns of cell pathology, progression rate, and regional vulnerability in vivo. *Neuron* 92, 796–812. doi: 10.1016/j.neuron.2016.09.055
- Kolarova, M., Sengupta, U., Bartos, A., Ricny, J., and Kaye, R. (2017). Tau Oligomers in Sera of Patients with Alzheimer's Disease and Aged Controls. *J. Alzheimers Dis.* 58, 471–478. doi: 10.3233/JAD-170048
- Kumar, S., Tepper, K., Kaniyappan, S., Biernat, J., Wegmann, S., Mandelkow, E.-M., et al. (2014). Stages and conformations of the tau repeat domain during aggregation and its effect on neuronal toxicity. *J. Biol. Chem.* 289, 20318–20332. doi: 10.1074/jbc.M114.554725
- Lasagna-Reeves, C. A., Castillo-Carranza, D. L., Guerrero-Muñoz, M. J., Jackson, G. R., and Kaye, R. (2010). Preparation and characterization of neurotoxic tau oligomers. *Biochemistry* 49, 10039–10041. doi: 10.1021/bi1016233
- Lasagna-Reeves, C. A., Castillo-Carranza, D. L., Sengupta, U., Guerrero-Munoz, M. J., Kiritoshi, T., Neugebauer, V., et al. (2012a). Alzheimer brain-derived tau oligomers propagate pathology from endogenous tau. *Sci. Rep.* 2:700. doi: 10.1038/srep00700
- Lasagna-Reeves, C. A., Castillo-Carranza, D. L., Sengupta, U., Sarmiento, J., Troncoso, J., Jackson, G. R., et al. (2012b). Identification of oligomers at early stages of tau aggregation in Alzheimer's disease. *FASEB J.* 26, 1946–1959. doi: 10.1096/fj.11-199851

- Li, W., and Lee, V. M.-Y. (2006). Characterization of Two VQIXXK Motifs for Tau Fibrillization in Vitro. *Biochemistry* 45, 15692–15701. doi: 10.1021/bi061422
- Lindberg, D. J., Wranné, M. S., Gilbert Gatty, M., Westerlund, F., and Esbjörner, E. K. (2015). Steady-state and time-resolved Thioflavin-T fluorescence can report on morphological differences in amyloid fibrils formed by A $\beta$ (1–40) and A $\beta$ (1–42). *Biochem. Biophys. Res. Commun.* 458, 418–423. doi: 10.1016/j.bbrc.2015.01.132
- Liu, C., and Götz, J. (2013). Profiling murine tau with 0N, 1N and 2N isoform-specific antibodies in brain and peripheral organs reveals distinct subcellular localization, with the 1N isoform being enriched in the nucleus. *PLoS One* 8:e84849. doi: 10.1371/journal.pone.0084849
- Lu, J., Li, T., He, R., Bartlett, P. F., and Götz, J. (2014). Visualizing the microtubule-associated protein tau in the nucleus. *Sci. China Life Sci.* 57, 422–431. doi: 10.1007/s11427-014-4635-4630
- Margittai, M., and Langen, R. (2004). Template-assisted filament growth by parallel stacking of tau. *Proc. Natl. Acad. Sci. U.S.A.* 101, 10278–10283. doi: 10.1073/pnas.0401911101
- Meier, S., Bell, M., Lyons, D. N., Rodriguez-Rivera, J., Ingram, A., Fontaine, S. N., et al. (2016). Pathological tau promotes neuronal damage by impairing ribosomal function and decreasing protein synthesis. *J. Neurosci.* 36, 1001–1007. doi: 10.1523/JNEUROSCI.3029-15.2016
- Meyer, V., Dinkel, P. D., Rickman Hager, E., and Margittai, M. (2014). Amplification of tau fibrils from minute quantities of seeds. *Biochemistry* 53, 5804–5809. doi: 10.1021/bi501050g
- Meyer, V., Holden, M. R., Weismiller, H. A., Eaton, G. R., Eaton, S. S., and Margittai, M. (2016). Fracture and growth are competing forces determining the fate of conformers in tau fibril populations. *J. Biol. Chem.* 291, 12271–12281. doi: 10.1074/jbc.M116.715557
- Michel, C. H., Kumar, S., Pinotsi, D., Tunnacliffe, A., George-Hyslop, P. S., Mandelkow, E., et al. (2014). Extracellular monomeric tau protein is sufficient to initiate the spread of tau protein pathology. *J. Biol. Chem.* 289, 956–967. doi: 10.1074/jbc.M113.515445
- Mohamed, N.-V., Herrou, T., Plouffe, V., Piperno, N., and Leclerc, N. (2013). Spreading of tau pathology in Alzheimer's disease by cell-to-cell transmission. *Eur. J. Neurosci.* 37, 1939–1948. doi: 10.1111/ejn.12229
- Murrell, J. R., Spillantini, M. G., Zolo, P., Guazzelli, M., Smith, M. J., Hasegawa, M., et al. (1999). Tau gene mutation G389R causes a tauopathy with abundant pick body-like inclusions and axonal deposits. *J. Neuropathol. Exp. Neurol.* 58, 1207–1226. doi: 10.1097/00005072-199912000-00002
- Narasimhan, S., Guo, J. L., Changolkar, L., Stieber, A., McBride, J. D., Silva, L. V., et al. (2017). Pathological tau strains from human brains recapitulate the diversity of tauopathies in non-transgenic mouse brain. *J. Neurosci.* 37, 11406–11423. doi: 10.1523/JNEUROSCI.1230-17.2017
- Rady, R. M., Zinkowski, R. P., and Binder, L. I. (1995). Presence of tau in isolated nuclei from human brain. *Neurobiol. Aging* 16, 479–486. doi: 10.1016/0197-4580(95)00023-28
- Rauch, J. N., Chen, J. J., Sorum, A. W., Miller, G. M., Sharf, T., See, S. K., et al. (2018). Tau Internalization is Regulated by 6-O Sulfation on Heparan Sulfate Proteoglycans (HSPGs). *Sci. Rep.* 8:6382. doi: 10.1038/s41598-018-24904-z
- Ritter, M. L., Avila, J., García-Escudero, V., Hernández, F., and Pérez, M. (2018). Frontotemporal dementia-associated N279K tau mutation localizes at the nuclear compartment. *Front. Cell. Neurosci.* 12:202. doi: 10.3389/fncel.2018.00202
- Sanders, D. W., Kaufman, S. K., DeVos, S. L., Sharma, A. M., Mirbaha, H., Li, A., et al. (2014). Distinct Tau Prion Strains Propagate in Cells and Mice and Define Different Tauopathies. *Neuron* 82, 1271–1288. doi: 10.1016/j.neuron.2014.04.047
- Sengupta, U., Portelius, E., Hansson, O., Farmer, K., Castillo-Carranza, D., Woltjer, R., et al. (2017). Tau oligomers in cerebrospinal fluid in Alzheimer's disease. *Ann. Clin. Transl. Neurol.* 4, 226–235. doi: 10.1002/acn3.382
- Sergeant, N., Delacourte, A., and Buée, L. (2005). Tau protein as a differential biomarker of tauopathies. *Biochim. Biophys. Acta* 1739, 179–197. doi: 10.1016/j.bbadis.2004.06.020
- Shammas, S. L., García, G. A., Kumar, S., Kjaergaard, M., Horrocks, M. H., Shivji, N., et al. (2015). A mechanistic model of tau amyloid aggregation based on direct observation of oligomers. *Nat. Commun.* 6:7025. doi: 10.1038/ncomms8025
- Sjöberg, M. K., Shestakova, E., Mansuroglu, Z., Maccioni, R. B., and Bonnefoy, E. (2006). Tau protein binds to pericentromeric DNA: a putative role for nuclear tau in nucleolar organization. *J. Cell Sci.* 119, 2025–2034. doi: 10.1242/jcs.02907
- Spillantini, M. G., and Goedert, M. (2013). Tau pathology and neurodegeneration. *Lancet Neurol.* 12, 609–622. doi: 10.1016/S1474-4422(13)70090-70095
- Stöhr, J., Wu, H., Nick, M., Wu, Y., Bhaté, M., Condello, C., et al. (2017). A 31-residue peptide induces aggregation of tau's microtubule-binding region in cells. *Nat. Chem.* 9, 874–881. doi: 10.1038/nchem.2754
- Strang, K. H., Croft, C. L., Sorrentino, Z. A., Chakrabarty, P., Golde, T. E., and Giasson, B. I. (2017). Distinct differences in prion-like seeding and aggregation between tau protein variants provide mechanistic insights into tauopathies. *J. Biol. Chem.* 293, 2408–2421. doi: 10.1074/jbc.M117.815357
- Sultan, A., Nessler, F., Violet, M., Bégard, S., Loyens, A., Talahari, S., et al. (2011). Nuclear Tau, a key player in neuronal DNA protection. *J. Biol. Chem.* 286, 4566–4575. doi: 10.1074/jbc.M110.199976
- Tepper, K., Biernat, J., Kumar, S., Wegmann, S., Timm, T., Hübschmann, S., et al. (2014). Oligomer formation of tau protein hyperphosphorylated in cells. *J. Biol. Chem.* 289, 34389–34407. doi: 10.1074/jbc.M114.611368
- Usenovic, M., Niroomand, S., Drolet, R. E., Yao, L., Gaspar, R. C., Hatcher, N. G., et al. (2015). Internalized tau oligomers cause neurodegeneration by inducing accumulation of pathogenic tau in human neurons derived from induced pluripotent stem cells. *J. Neurosci.* 35, 14234–14250. doi: 10.1523/JNEUROSCI.1523-15.2015
- von Bergen, M., Barghorn, S., Biernat, J., Mandelkow, E.-M., and Mandelkow, E. (2005). Tau aggregation is driven by a transition from random coil to beta sheet structure. *Biochim. Biophys. Acta* 1739, 158–166. doi: 10.1016/j.bbadis.2004.09.010
- von Bergen, M., Barghorn, S., Li, L., Marx, A., Biernat, J., Mandelkow, E.-M., et al. (2001). Mutations of tau protein in frontotemporal dementia promote aggregation of paired helical filaments by enhancing local  $\beta$ -structure. *J. Biol. Chem.* 276, 48165–48174. doi: 10.1074/jbc.M105196200
- von Bergen, M., Friedhoff, P., Biernat, J., Heberle, J., Mandelkow, E.-M., and Mandelkow, E. (2000). Assembly of  $\tau$  protein into Alzheimer paired helical filaments depends on a local sequence motif (306VQIVYK311) forming  $\beta$  structure. *Proc. Natl. Acad. Sci. U.S.A.* 97, 5129–5134. doi: 10.1073/pnas.97.10.5129
- Walsh, D. M., and Selkoe, D. J. (2016). A critical appraisal of the pathogenic protein spread hypothesis of neurodegeneration. *Nat. Rev. Neurosci.* 17, 251–260. doi: 10.1038/nrn.2016.13
- Wang, Y., and Mandelkow, E. (2016). Tau in physiology and pathology. *Nat. Rev. Neurosci.* 17, 22–35. doi: 10.1038/nrn.2015.1
- Wegmann, S., Maury, E. A., Kirk, M. J., Saqran, L., Roe, A., DeVos, S. L., et al. (2015). Removing endogenous tau does not prevent tau propagation yet reduces its neurotoxicity. *EMBO J.* 34, 3028–3041. doi: 10.15252/embj.201592748
- Wong, A. G., Wu, C., Hannaberry, E., Watson, M. D., Shea, J.-E., and Raleigh, D. P. (2016). Analysis of the amyloidogenic potential of pufferfish (takifugu rubripes) islet amyloid polypeptide highlights the limitations of thioflavin-T assays and the difficulties in defining amyloidogenicity. *Biochemistry* 55, 510–518. doi: 10.1021/acs.biochem.5b01107
- Wu, J. W., Herman, M., Liu, L., Simoes, S., Acker, C. M., Figueroa, H., et al. (2013). Small misfolded Tau species are internalized via bulk endocytosis and anterogradely and retrogradely transported in neurons. *J. Biol. Chem.* 288, 1856–1870. doi: 10.1074/jbc.M112.394528
- Yin, Y., Gao, D., Wang, Y., Wang, Z.-H., Wang, X., Ye, J., et al. (2016). Tau accumulation induces synaptic impairment and memory deficit by calcineurin-mediated inactivation of nuclear CaMKIV/CREB signaling. *Proc. Natl. Acad. Sci. U.S.A.* 113, E3773–E3781. doi: 10.1073/pnas.1604519113

**Conflict of Interest Statement:** The authors declare that the research was conducted in the absence of any commercial or financial relationships that could be construed as a potential conflict of interest.

Copyright © 2019 Karikari, Nagel, Grainger, Clarke-Bland, Crowe, Hill and Moffat. This is an open-access article distributed under the terms of the Creative Commons Attribution License (CC BY). The use, distribution or reproduction in other forums is permitted, provided the original author(s) and the copyright owner(s) are credited and that the original publication in this journal is cited, in accordance with accepted academic practice. No use, distribution or reproduction is permitted which does not comply with these terms.